BERGISCHE
UNIVERSITÄT
WUPPERTAL

University of Wuppertal
Department of Computer Simulation for Fire Safety and Pedestrian Traffic
Degree Program Safety Engineering

Agent-based modelling for crowding and queuing in front of bottlenecks

Master Thesis

Supervisors:

Prof. Dr. Armin Seyfried
Dr. Mohcine Chraibi

submitted by:

Ben Hein

Wuppertal, April 2019

Even if a scientific model, like a car, has only a few years to run before it is discarded, it serves its purpose for getting from one place to another.

- David L. Wingate

Abstract

The current design of concert and festival entrances shows a great variety, the occurrence of bottlenecks being inevitable. Recent experimental research shows that safety considerations for such scenarios are necessary as factors like corridor width, number of people and motivation of the latter have an impact on the occurrence of queuing and crowding and the resulting density in front of the bottleneck. As the behaviour of such systems with respect to the above-mentioned factors is unclear, velocity-based microscopic modelling and simulation is used as a means of abstraction to understand the underlying mechanisms to a greater extent.

The results show that queuing and crowding phenomena can be reproduced in different corridor widths, the essential influence on density increase being the geometric boundary condition, which changes the desired directions of agents. This raises interaction and negotiation issues and makes phenomena such as overtaking, space filling and blocking occur with increasing corridor width. By changing the contraction time scale of the crowd in the simulation, the dissolving of ordered structures is observed leading to a further overall density increase. This is much more pronounced in a narrow corridor, which still results in lower densities due to a boundary effect around walls. Finally, runaway values observed in the experiment can be explained by means of simulation results.

Thus, velocity-based modelling and simulation make these specific bottleneck setups found in the real world more comprehensible and pave the way for future extensions to the original model to further investigate the complexity of such scenarios.

Declaration

I declare that I have authored this thesis independently, that I have not used other than the declared sources/resources, and that I have explicitly marked all material which has been quoted either literally or by content from the used sources.

Wuppertal, April 2019 Ben Hein

Contents

List of Figures

List of Tables

Chapter 1

Introduction

1.1 Background

Mass events like concerts or festivals assemble specific geometric designs with the use of barriers to split and regulate incoming pedestrian flows. At some point, these entrance scenarios result in a bottleneck making safety aspects matter. Understanding the interaction between infrastructure and people is therefore a crucial aspect in order to design a safe entrance system.

In this context, several types of real-world entrance setups were already tested and observed in experiments [3, 2]. Experimental data for bottlenecks shows that a specific entrance system can lower the occurrence of pushing among people forced to wait. Furthermore, factors like corridor width, number of participants and motivation have an impact on whether queuing or crowding behaviour and an accompanying high density in front of the bottleneck occurs. In general, this density increase is accomplished by broadening the corridor and by raising the motivation of the participants, but the population size also appears to affect the pushing occurrence and density reached. [3]

1.2 Problem statement

The reasons for the above-mentioned behaviour of these systems are however unknown, which makes it hard to derive meaningful correlations. Mainly, the established width-density relations through numerous experimental runs are of great interest.

Having this in mind, the goal of this thesis focuses on studying this real-world system by means of abstraction in order to get a basic grasp on the experimental data and possibly identify key influence factors. This is realised by conducting static pre-analyses and making use of agent-based modelling and simulation. For this, an

appropriate modelling environment in the form of a simple operational model as well as suitable model parameters need to be set up to reproduce the pedestrian dynamics found in the experiments with focus on phenomena like queuing and crowding as well as width-density correlations. This includes finding approaches for setting up initial conditions, identifying model parameters like an agent's motivation and the definition of different types of agents regarding their behaviour. Furthermore, the subsequent variations of corridor width, number of agents and motivational states in the form of various simulation runs need to be handled. On the other hand, evaluation of the ability of the used model to reproduce the observed pedestrian dynamics in the first place are possibly necessary, which leads to detecting future implementations for the original model. Ultimately, the analyses made in this thesis should shed light on the experimental data gathered and somewhat elucidate real-world pedestrian dynamics in front of bottlenecks.

1.3 Outline of this thesis

To give a general overview, Chapter 2 begins by a short literature review of the 21st century concerning research of crowd behaviour in front of bottlenecks. The state of the art section goes on with defining specific measurement methods for flow and density of pedestrian dynamics and tries to clarify what is currently understood by queuing and crowding. In a further step, the aspect of pushing is broken down. These general explanations are then followed by two experimental setups to introduce the particular research. The experimental data gathered from one of these setups will be used for comparison with the simulation results, the main part of this thesis. Therefore, the state of the art section includes motivating aspects for modelling and simulation as well. Moreover, possible modelling approaches are discussed shortly and reasons given for making use of a velocity-based model. The governing equations of the used collision-free speed model are given and the JuPedSim framework, to which this model belongs, introduced.

Chapter 3 concentrates on preliminary work such as filtering and fitting the experimental data set to exclude parameters that were not controlled during the experiment. The section also includes the setting up of different geometries and studying the effect of these geometries on maximum densities and maximum neighbours by defining two different configurations of circle arrangement. As for the simulation scenarios, initial conditions like initial agent distribution and accompanying densities as well as model parameters setting are discussed. Specifically the use of calibration parameters and

agent parameters to reproduce motivation and the definition of two types of agents is addressed. Further configuration steps of simulation input files, generation of the necessary file structure and the general automated work flow for simulation complete this chapter.

Chapter 4 starts with the results presentation for the corridor width variation by means of Voronoi diagrams, time-density series, width-density relations in a specific time interval, trajectory analysis, comparison between individual distance to target and time to target and further self-implemented analyses. This is followed by the results of the number of agents variation and a specific test scenario to demonstrate an unexpected model behaviour. Finally, results for the variation of motivation are presented. The section terminates by a thorough discussion of all results, sets these into an overall scientific context and addresses possible and necessary model extensions.

The last Chapter 5 gives a summary of the results obtained to draw conclusions and a short outlook.

Chapter 2

State of the art

2.1 Pedestrian research in front of bottlenecks

The Encyclopedia of Complexity and Systems Science [5] defines a bottleneck as "a part of facility limiting pedestrian flows. This can be, for example, a door, a narrowing in a corridor, or stairs, i.e., locations of reduced capacity. At bottlenecks jamming occurs if the inflow is higher than the capacity, which is the maximal flow rate supported by a facility." The physical quantities like flow rate and density are defined in the measurement methods section.

During the last two decades diverse research regarding pedestrian dynamics in front of bottlenecks was done, mainly concerning pedestrian behaviour and the emergent flow. In 2001, Helbing [7, 8] reports self-organization phenomena of pedestrians at bottlenecks by observing oscillations in the passing direction in bi-directional flows. Nagatani [9, 10] points out the dynamical transition and scaling behaviour of pedestrian flows at a bottleneck.

In 2005, Hoogendoorn and Daamen [11, 12] report that pedestrians inside bottlenecks form layers, the number of layers augmenting with the width, however that "the life span of these layers is rather small" [11] in wide bottlenecks. Furthermore, several walking patterns in narrow corridors are identified, which indicate lane behaviour. They also discuss that aside from the width and wall surface of a bottleneck, the interaction behaviour of the pedestrians passing the bottleneck is important and use the zipper effect to explain the stepwise increase of the capacity of a bottleneck. [11, 12]

In 2006, Kretz [13] shows that the specific flux declines linearly with increasing width of the bottleneck with the condition of only one person passing at a specific time, otherwise the flux is constant for larger bottleneck widths. In 2009, Seyfried [1] reports a linear growth of pedestrian flow with the bottleneck width, which results in

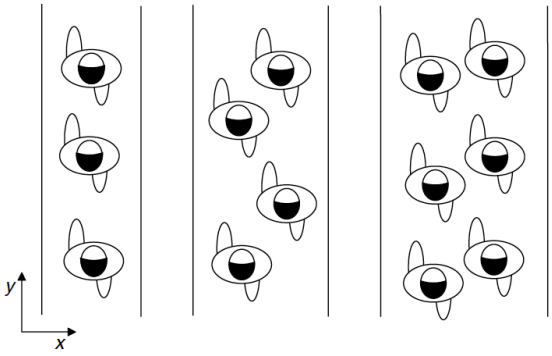

Figure 2.1: Zipper effect with increasing width and thus distance between lanes augmenting [1]

the capacity estimation for bottlenecks being revised. The density increase in front of the bottleneck is explained with the zipper effect in combination with boundary effects, which is shown in figure 2.1. It is elaborated that as the space at boundaries cannot be used as efficiently as in the center of the bottleneck, the density will increase for greater widths [1].

In the following years, these density-specific investigations together with jam analysis in front of bottlenecks came to the fore as these considerations are likewise necessary in order to design a safe infrastructure. Before going into more particular experimental studies, a short overview of flow and density measurement is given.

2.2 Measurement methods

The flow rate in a time interval T [14] is defined by:

$$J = \frac{\Delta N}{T} \tag{2.1}$$

where ΔN is the difference in agents passed. Other possibilities to measure the flow are the inverse mean of time gaps between two consecutive pedestrians or the hydrodynamic relation [14] in the form of:

$$J = \rho \cdot v \cdot w \tag{2.2}$$

where w is the width for which the flow rate is determined, v and ρ the average speed and density of a pedestrian stream. The occurrence of jamming will ultimately result in a density increase. The density measurement in front of a bottleneck can be measured in several ways from which one is the arithmetic mean of all agents N in a defined

measurement area A:

$$\rho = \frac{N}{A} \tag{2.3}$$

A second approach is to calculate individual Voronoi cells [15]. These are constructed with respect to their origin, which are people or agents in our case. A Voronoi cell contains all points in space nearer to its origin than any other origin. This results in an area of points, the individual area that is available to a person or agent. From this area A_{ind}, the individual Voronoi density ρ_{ind} can be calculated by:

$$\rho_{ind} = \frac{1}{A_{ind}} \tag{2.4}$$

If the Voronoi density has to be calculated in a specific measurement area A_{ma} containing several Voronoi cells, the individual Voronoi densities have to be integrated with respect to the geometric boundaries as well as averaged:

$$\rho_{ma} = \frac{\iint \rho_{ind}\, dx\, dy}{A_{ma}} \tag{2.5}$$

Figure 2.2 shows an exemplary Voronoi diagram with several cells. Advantages of the Voronoi density are high resolution and lower standard deviations in comparison to other density measurement methods [16].

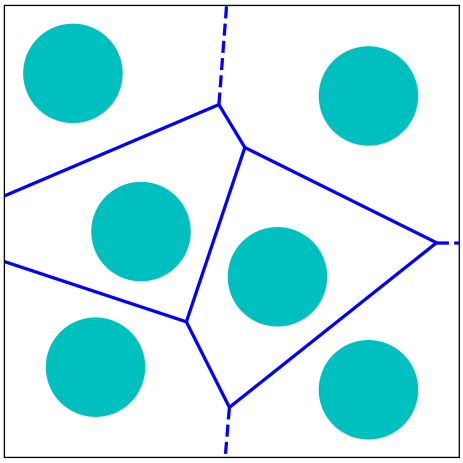

Figure 2.2: Exemplary Voronoi diagram. Light blue circles are pedestrians, dark blue lines indicate the Voronoi cells, which are infinite in the case of a dashed line as this representation is only a cutout

2.3 Differencing queuing, crowding and pushing

The verb queuing derives from the noun queue by which ”a line or sequence of people awaiting their turn to proceed” [17] is understood. The central element is the aspect of waiting from which waiting lines result. [17] Lane formation can be the cause of queuing.

The verb crowding derives from the noun crowd and is a term used in social psychology to describe this type of mass phenomena [18]. Generally, a large number of people make up a crowd in which the individuals can be gathered closely together or even move too close together so that spaces are almost filled completely. This state leaves little or no room for movement and can be described sociologically by the subjectively perceived constriction and intrusion into private space due to spatial limitations. The physical or spatial correlate is the objectively measurable density, the area available for one person, or the constraint of not being able to move freely. Thus a ”tightly packed mass” [17] is formed by clustering or congregating, the latter term interestingly originating from middle English senses like ”moving by pushing” or ”push one’s way” [17]. The aftermath of crowding includes stress and loss of control. [19, 17]

With regards to pushing, the state of knowledge insists that pushing occurs for a specific reason. As put clear by Henein [20], ”People in crowds do not push randomly [...]”, but ”push in a particular direction when they want to move in that direction and are prevented from doing so.” Helbing observes that the difference between the desired speed and the speed of the preceding pedestrian is linked to the distance that pedestrians keep from one another [7] and maintaining personal space in a crowd is a reason too [20]. As people want to move towards certain goals, they will be deflected by pushing, which are physical forces [21]. However, forces are not instantaneous but location-specific and combine additively before they can propagate through a crowd just like a shock wave [20]. Thus, factors that may influence pushing should be investigated. Two essential experiments with focus on analysing such pedestrian behaviours at entrance scenarios typically found at concerts and festivals are described in-depth below.

2.4 Experimental studies

2.4.1 Setup I

The general methodology of the experiments depicted in the following is recording video footage from above the participants using permanently installed GoPro cameras. Subjects receive coloured caps, which set clearly recognizable accents in the video

recordings. The footage is processed afterwards in a frame per frame manner with the software PeTrack, which was specifically developed at Jülich Research Centre. For supplementary information, a look at [22] should be taken. This software recognizes and tracks the cap markers and extracts trajectories from the individual positions and outputs files that can be further processed. For this, the module *JPSreport* from the software package JuPedSim can then be used to analyse the data [23, 24].

In 2013, the first set of experiments [2] showed that the spatial structure of barriers in entrance scenarios influences the density in front of the bottleneck. The aim was to find out whether and which rules of conduct apply and when these rules are addressed. The two setups were a semi-circle and a corridor scenario with guiding barriers from the side in front of two entrances. Both scenarios with participants are shown in Figure 2.3. In both cases, the participants were distributed loosely so that initial densities are comparable. Furthermore, the participants were motivated by telling them to be one of the first to pass through one of the entrances.

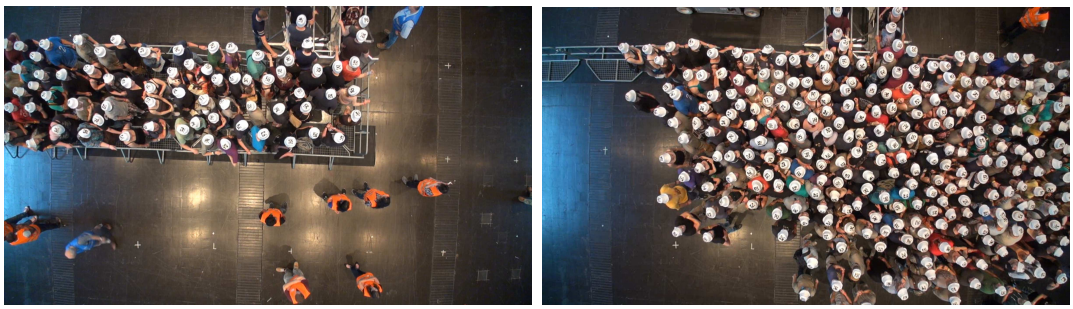

(a) corridor setup **(b)** semi-circle setup

Figure 2.3: Momentary pictures during experimental runs in June 2013 [2]

The results show higher Voronoi densities in front of the entrances in the semi-circle setup and a star-like pattern, whereas the corridor scenario results in ordered lanes. The semi-circle setup shows participants clearly filling spaces, moving as closely as possible and pushing behaviour as well.

However, the geometric constraints of both setups in the experiment in terms of width are not comparable and the produced motivation could blend the findings as it was not a controlled parameter. Furthermore, these experiments did not use a constant measurement area as different rectangular measurement areas, 3 by 1 meters for the semi-circle and 2.3 by 1 meter to fit the boundaries of the corridor, were used.

2.4.2 Setup II

In 2018, another set of experiments [3] with varying corridor widths and using a variation of motivation was designed and its effects on the density in front of the bottleneck studied. These were realised on multiple days at the University of Wuppertal in January 2018. The runs were varied in such a way that on the one hand the corridor width was changed among five widths between 1.2 m and 5.6 m and on the other hand participants were given a low or high motivation to reach the entrance. The low motivation was generated by telling all participants that the front row had enough space for everyone. To intensify the motivation, the participants were told that only a restricted number of standing places for a good view were available. Four specific experimental views from above are shown in Figure 2.4.

A thorough analysis of the results has been made in [3]. Figure 2.5 shows selected time-density series from the experiment with a time window of t = 3 s. The curves are only smoothed to enhance a better distinction. Two main observations can be made: for identical motivations, the maximum density in front of the bottleneck increases with the corridor width and for increasing motivation an overall density increase is seen.

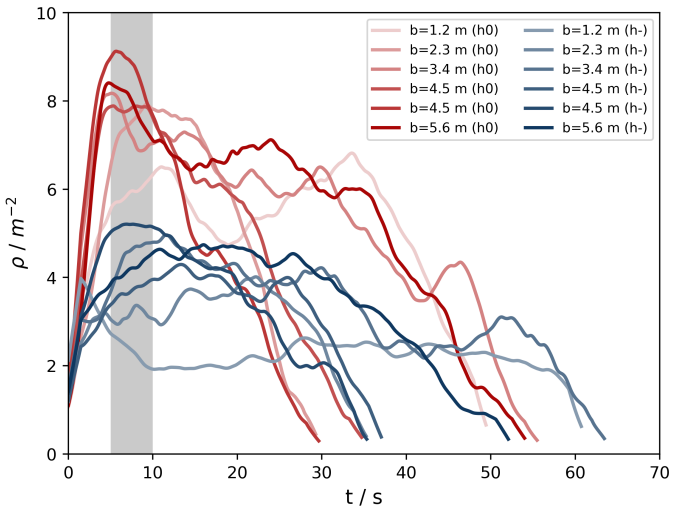

Figure 2.5: Time-density series for selected runs, low motivation being blue and high motivation red, time window t = 3 s

However, other factors like the varying number of participants significantly influences the occurrence of pushing and the level of density too [3]. The derived width-density relation, for which a density mean in the interval of 5 s to 10 s was considered, is shown in the next section as it will be further processed and used to compare the simulations to.

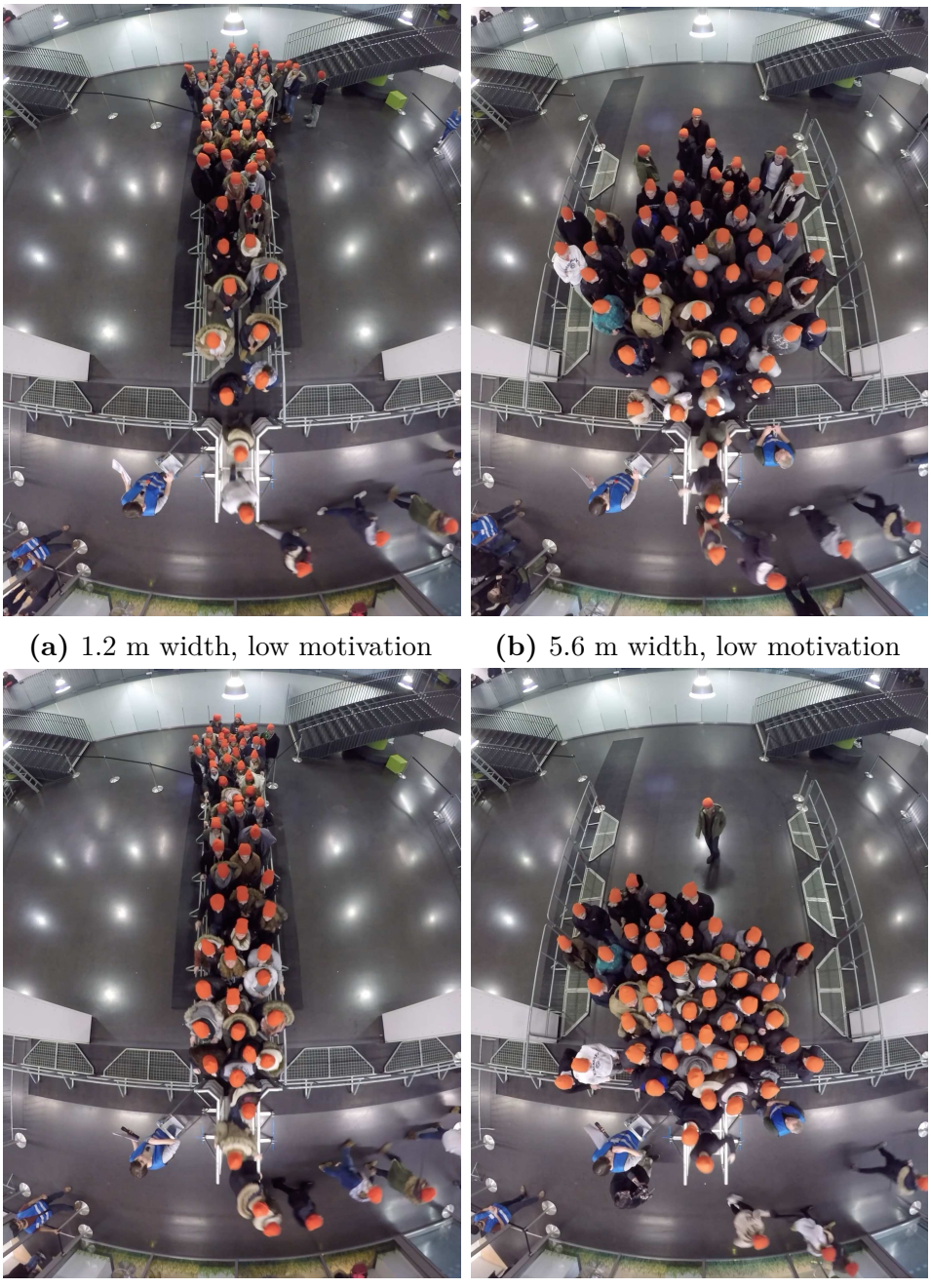

(a) 1.2 m width, low motivation **(b)** 5.6 m width, low motivation

(c) 1.2 m width, high motivation **(d)** 5.6 m width, high motivation

Figure 2.4: Momentary pictures during experimental runs in January 2018 for narrow and wide corridor with low and high motivation [3]

Thus, a guiding system in front of the entrance in the form of a narrow corridor seems to reduce pushing of the waiting people. A narrow corridor width appears to favour lane arrangement and force the participants into queues so that the densities occurring at the entrance are significantly lower. At wider widths, density in front of the entrance increases and crowding occurs. The transition between these two arrangements is observed between a corridor width of 1.2 m and 2.3 m. This however changes when intensifying the participants' motivation as pushing behaviour occurs and higher densities are reached. [3]

Furthermore, the experiment was able to identify two types of people. This is shown in figure 2.6 for a corridor width of 5.6 m and high motivation. Basically, participants opted for (or were forced to) either staying and waiting or moving fast and filling spaces. When a contracted stage is reached, pushing takes place. Figure 2.6 gathers the spatio-temporal dimensions of pushing as a thick branch.

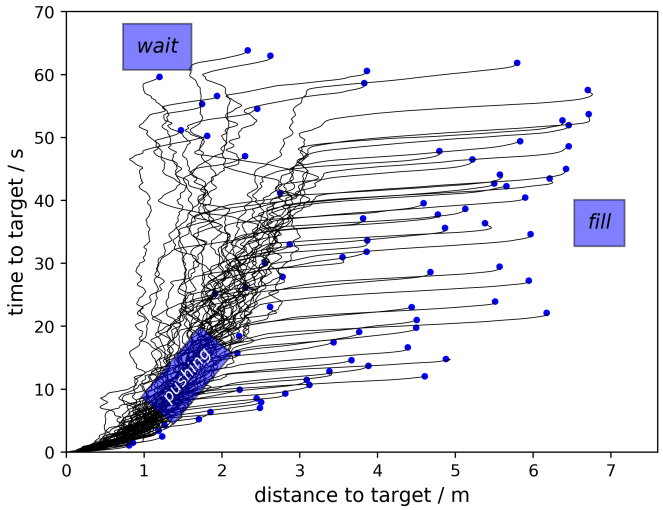

Figure 2.6: Two types of participants in the form of waiting and filling behaviour

2.5 Agent-based modelling

2.5.1 General motive for modelling

Studying any real system to better understand it involves coming up with a suitable model for this system. The overall process is shown in figure 2.7. Based on the experimental observations, a systematic model approach thus has to be found. This includes the mathematical description of the system by setting up required equations

and relevant parameters. Meanwhile, lots of model classes exist to map a real system for a particular purpose and most of the time mixed forms occur. After the model has been set up, its behaviour can then specifically be influenced and analysed by simulation. The data from observed and modelled behaviour can then be compared for further analysis. This can finally lead to future changes and improvements of the model in the form of a design cycle. It should however be clear that the model is always a rough approximation with the goal of modelling desired behaviour, so that the original system and the model can never be compared directly. [25, 4]

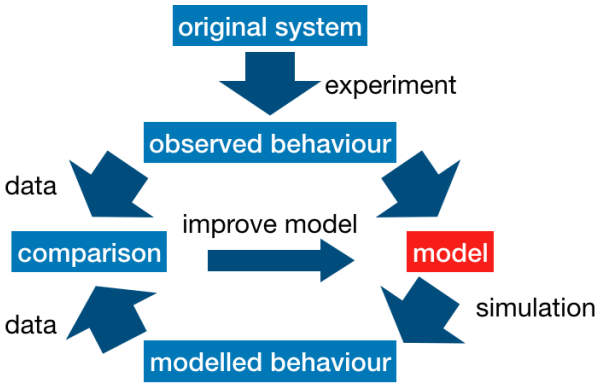

Figure 2.7: Process and use of modelling, derived from [4]

Nevertheless, models need to be accurate. The experimental results show that under different motivational conditions, pushing behaviour occurs. In this context, Henein and Shiwakoti [21, 20] insist on the fact that "force effects can cause them (people) to be pushed away from their desired trajectories and accurate models must reflect this. Also, the presence of crowd members injured by excessive force can significantly affect the ability of others to move freely. Models that do not represent pushing forces therefore cannot directly account for all these additional causes of delay." Furthermore, "it is essential to note [...] when modelling force [...] that force applied by individuals in one part of a modelled crowd must propagate through that crowd with certain time characteristics". In 2012, Ezaki [26] for instance used inflow and competitiveness parameters to simulate congested situations at bottlenecks.

2.5.2 Approaches for pedestrian dynamics

This thesis will focus on microscopic modelling, which represents pedestrians as stand-alone individuals that interact locally. This modelling approach is able to produce complex self-organisation phenomena with powerful pedestrian dynamics by implement-

ing simple models. However, thorough simulation analysis is necessary in order to fully grasp the relations between the emergence of these phenomena and the constructed model parameters. [5, 6]

Microscopic models can be further classified as continuous or discrete with regard to time and space as well as other state variables as is shown in figure 2.8. Further subcategories are related to a stochastic or deterministic character of the model and to what extent the operational model describes the movement of the agents in the simulation. On the one hand, force-based models use Newtonian dynamics by describing particles with inertia. One well-known representative is the social force model by Helbing [27], which uses three force terms to describe the acceleration towards the desired velocity, desired distance from other pedestrians and borders as well as attractive effects. Besides force-based models, there is the category of velocity-based models. [5, 28]

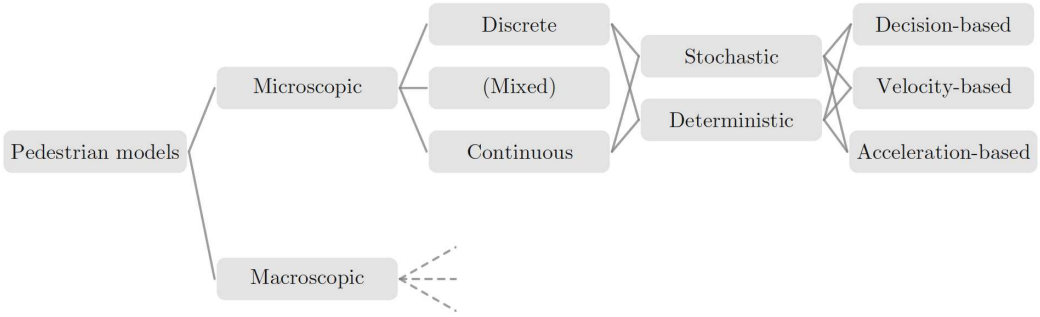

Figure 2.8: Possible classification for microscopic models [5]

In these models, agents visually consider their neighbourhood and use techniques to avoid collisions. The velocity is modelled via first-order differential equations and adjusted instantaneously without any reaction time. The velocity can be impeded to exclude particle collision and overlapping, which makes them reliable in modelling high densities. Moreover, less parameters and calibration of the latter are needed, making these models simpler to understand. Last but not least, a significant reduction of the computational effort is accomplished when comparing to force-based models. Therefore, a very minimal operational model in the form of a collision-free speed model is used to simulate the motion of agents in this thesis and compare them to the experimental data. [5, 6]

2.5.3 Velocity-based modelling

In this section, the governing equations of the used model are shown [6]. The velocity in this model is given by a scalar speed and a normalized direction:

$$\dot{\mathbf{x}}_\mathbf{i} = V(s_i(\mathbf{x}_i, \mathbf{x}_j, \dots)) \times \mathbf{e}_i(\mathbf{x}_i, \mathbf{x}_j, \dots) \tag{2.6}$$

in which the first term represents the optimal speed function and e_i the moving direction. Both the speed and the direction of an agent depend on the relative positions of their neighbours.

e_i is the direction model and is given by a simplified version of the additive form of the gradient navigation model, where a repulsion function is used depending on the distances $s_{i,j}$ with neighbours:

$$\mathbf{e}_i(\mathbf{x}_i, \mathbf{x}_j, \dots) = \frac{1}{N}(\mathbf{e}_0 + \sum_j (\mathbf{R}(s_{i,j}) \cdot \mathbf{e}_{i,j}) \tag{2.7}$$

with e_0 the desired direction, N a normalization constant in order to obtain a unit vector and $R(s_{i,j})$ the repulsion function given by:

$$R(s_{i,j}) = a \cdot exp\left(\frac{-s_{i,j}}{D}\right) \tag{2.8}$$

where $s_{i,j}$ is the spacing distance between pedestrians i and j, a the repulsion rate and D the repulsion distance (e.g. range). The minimal spacing s_i is then calculated among the set J_i of pedestrians with a size of diameter l in front of a given pedestrian i by:

$$J = \{j, e_i \cdot e_{i,j} \leq 0 \text{ and } |e_i{}^{\perp} \cdot e_{i,j}| \leq l/s_{i,j}\} \tag{2.9}$$

For a better understanding, this set is represented in figure 2.9.

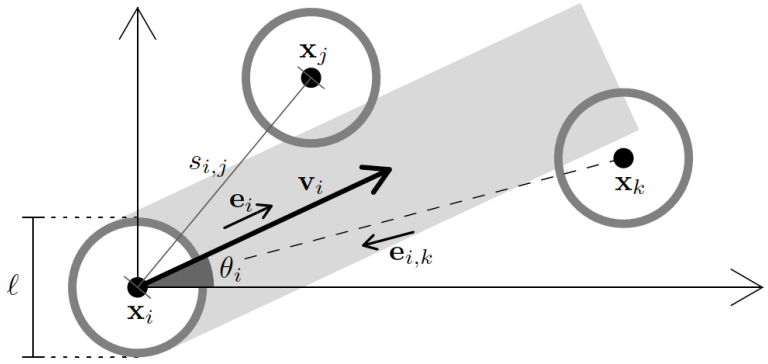

Figure 2.9: Set of pedestrians for calculating minimal spacing in front [6]

The minimum distance in front is then given by:

$$s_i = min_{j \in J_i} s_{i,j} \tag{2.10}$$

As the optimal speed function is given by the piecewise linear function:

$$V(s_i) = min\{v_0, max\{0, (s_i - l)/T\}\} \tag{2.11}$$

the speed depends on the desired speed v_0, the minimal spacing in front s_i, the pedestrian diameter l and the time gap T.

This operational model is part of *JPScore*, one module of the software package JuPedSim [23] developed at Jülich Research Centre. The JuPedSim framework is focused on academic use and implements sub-models for researching particular pedestrian dynamics. The program code itself is mainly written in C++. *JPScore* has no graphical user interface and can only be executed in shell-mode, thus all input and output files are .xml or .txt based.

JPScore computes the trajectories based on an initial configuration file and using a geometry file. The latter can be set up and edited using a provided editor. The initial configuration file needs several specifications, from which one is the operational model to describe the pedestrians movement in space. On the tactical level, several route choice models exist, depending on whether a navigation graph based on graph theory and made up of nodes and edges or a generated floorfield is used. Route choice patterns like shortest and global shortest path as well as quickest path are possible. On a strategic level, a direction strategy is specified, which defines the desired direction of a pedestrian and is router dependent. Furthermore, the initial configuration file takes general frame conditions like maximum simulation time and a seed. Basically, different seeds engender different initial conditions like spatial agent distribution and characteristics with the purpose of randomisation. More details can be found online at `http://www.jupedsim.org`.

The module *JPSvis* can be used for visualizing the outputted trajectory files and *JPSreport* for different analyses of the computed trajectories. This thesis uses a build of *JPScore* version 0.8.4 and *JPSreport* version 0.8.3.

Chapter 3

Preliminary work and methodology

3.1 Filtering and fitting data set

As shown for the setup II experiment, density in front of the bottleneck generally increases by widening the corridor and by intensifying the motivation of the participants, but the number of participants seems to influence the level of density as well. If the number of participants is low, low densities are measured even when the motivation is high. On the other hand, high densities are measured with a high number of participants, but a low motivation. Figure 3.1 shows the experimental data for all runs.

In order to account for this significant impact of the number of participants N and ensure comparability when putting experimental and simulation results side by side, a selection of the experimental data is made. This should at least filter possible effects due to the size of the population. Therefore, all runs not fulfilling $N \in [30, 70]$ are discarded, by which rather low (< 30 participants) and high populations sizes (> 70 pedestrians) are eliminated. These thresholds can of course be selected differently. In this case, the 8 runs 030, 040, 070, 080, 170, 180, 190 and 200 [3] are eliminated. The mean and median of the remaining data are:

$$\bar{N} = 52.16$$

$$\tilde{N} = 49.5$$

It is noticed that there is a general increase in the density, but that the density asymptotes towards a maximum. A standard model for this sort of asymptotic function or a saturation curve is an exponential. In order to better describe the data and possibly track down differences, negative exponential growth functions of the form:

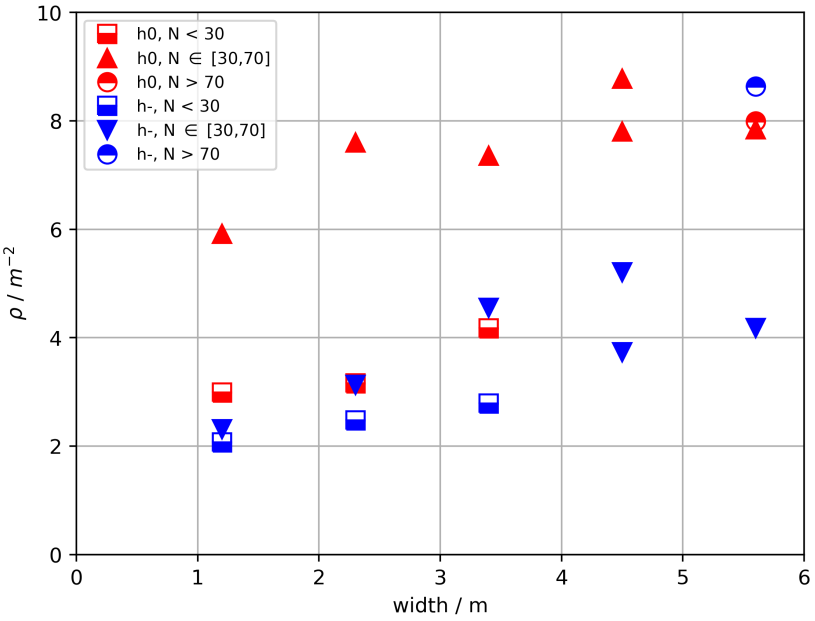

Figure 3.1: calculated mean density ($t \in [5-10]s$) data differentiated by number of participants and motivation (h- = low, h0 = high)

$$f(x) = a \cdot (1 - e^{-b \cdot x}) \tag{3.1}$$

have been fitted with the least squares method to the experimental data represented in figure 3.2, with parameter a representing the maximum density reached and parameter b the steepness and thus a sort of "duration" to reach it. The correlation index for both variables is calculated and given in table 3.1.

motivation	**a**	**b**	**correlation index**
low	4.73	0.57	-0.881
high	8.06	1.11	-0.633

Table 3.1: Exponential functions describing the low and high motivation curves with their respective correlation index

It can be seen that the correlation index for both variables in the low motivation curve is negative and rather high, which means that the maximum density takes longer to reach. For high motivation, the correlation between both variables is negative as well but lower, which indicates that the maximum density is achieved earlier. The fit for the high motivation data shows indeed that the maximum density is reached quickly.

However, to clarify, these curves were only fitted to deduce possible differences

within the data sets of low and high motivation. The curves can of course be of another form, especially the high motivation curve may not be exponential, but rather a constant function with a kink at the beginning. The low motivation curve could also be a linear function. However, the used fits give the insight of maximum density being reached faster with high motivation, whereas it is reached gradually for a low motivation. Furthermore, the process of filtering and fitting shows the influence of corridor width, number of participants and motivation in a more explicit way.

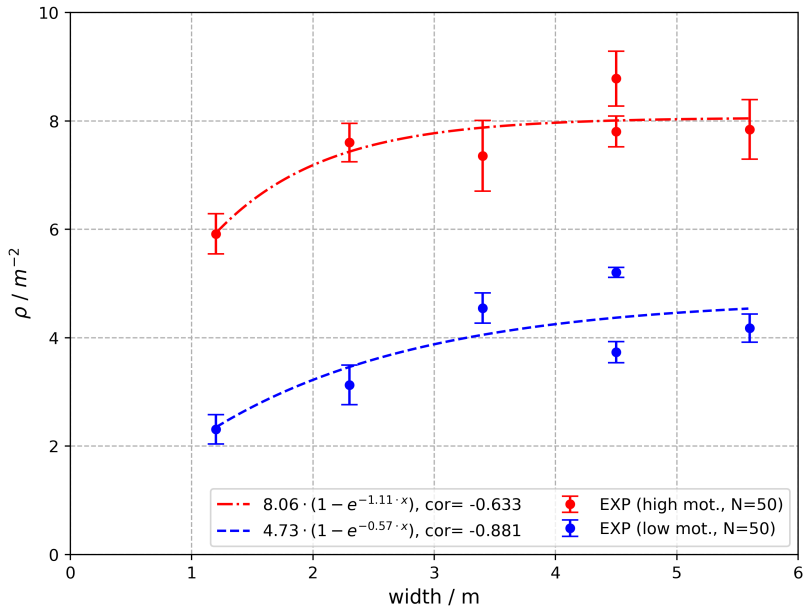

Figure 3.2: Resulting exponential curves from fitting selected experimental data, mathematical expressions of functions are given in the legend

3.2 Analysis of geometric boundary conditions

A general density increase is seen irrelevant of the motivation and number of participants, which puts forward the impact of corridor width. Therefore, the following passages account for physical boundary effects due to specific circle radius r and corridor width w interaction, which could possibly discretize the maximum density in front of the bottleneck. This is done via analysis of maximum packing densities of identical circles with the assumption of pedestrians being circles, when in reality a better description can be made with ellipses.

In order to analyse different corridor widths, one main symmetric geometry is build.

This geometry can be adapted to give a certain corridor width and is shown in figure 3.3

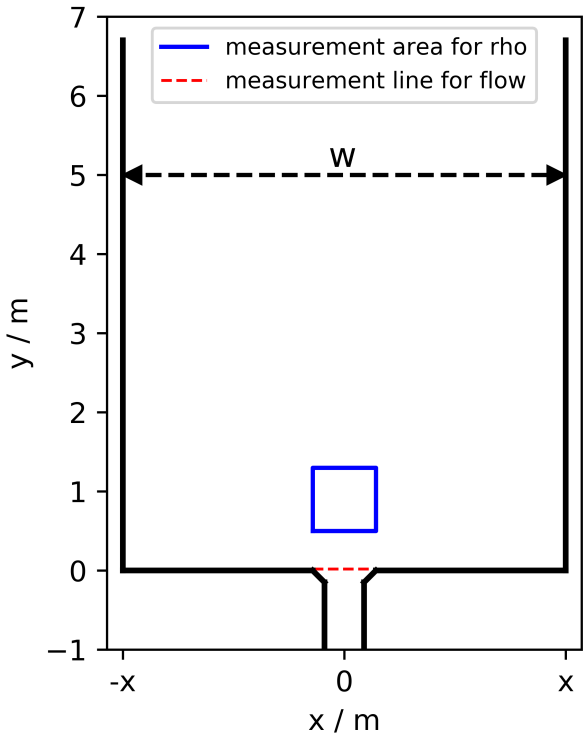

Figure 3.3: Dummy geometry for all scenarios in this thesis, the blue square is used for density measurement, the red dashed line for flow measurement

The coordinate in x-direction is adapted to get the specific corridor width by planting the values from table 3.2. The exit has a width of 0.5 m. An exemplary geometry inifile is given in the appendix A.

Table 3.2: x-values for producing specific geometries

width w	1.2 m	2.3 m	3.4 m	4.5 m	5.6 m
x coordinate	0.60 m	1.15 m	1.70 m	2.25 m	2.80 m

In order to analyse maximum packing densities, two different possible configurations in the form of square packing and hexagonal packing are defined. For the configuration definition, adapted calculations from Prof. Dr. Bernhard Steffen (TU Dortmund) are used.

For both configurations, the arrangement in y-direction is periodically as there is no limitation by walls. The y-coordinates of the circles of the i-th row are given by:

$$y_i = i \cdot r + (i-1) \cdot h \tag{3.2}$$

where h is the height between the highest point of the first row and the center of the second row and specific to the configuration. As for the arrangement in x-direction, the width w is the constraint. In a square packing, all rows contain N circles, whereas in a hexagonal packing, uneven rows contain N and even rows N-1 circles. Generally, the maximum number of circles N that is possible in a row is given by:

$$N = int\left(\frac{w}{2r}\right) \tag{3.3}$$

The calculation for the x-coordinates and h is done configuration-wise in the following. As for configuration 1, all rows contain N circles. In order to guarantee for a dense packing, several calculations are necessary for h_1 and x_i. The free space d_1 in a row is given by:

$$d_1 = w - 2 \cdot r \cdot N \tag{3.4}$$

Two different cases then need to be looked at. If $d_1 < r$, there is no space in between the circles as represented in figure 3.4 and h_1 is given by:

$$h_1 = \sqrt{4 \cdot r^2 - d_1^2} - r \tag{3.5}$$

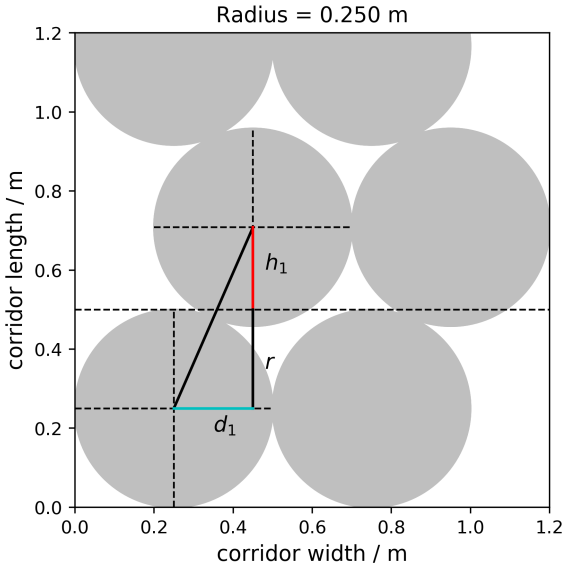

Figure 3.4: Reference lines and distances for configuration 1 (square) in order to calculate height h_1 if $d_1 < r$

The x-coordinates for uneven (see 3.6) and even rows (see 3.7) are then given by:

$$x_i = r \cdot (2 \cdot i + 1), i = 0 \dots N - 1 \tag{3.6}$$

$$x_i = r \cdot (2 \cdot i - 1) + d_1, i = 1 \dots N \tag{3.7}$$

If $d_1 > r$, there is a distance between the circles. This can be expressed as $d_{between}$, which is graphically shown in figure 3.5. Mathematically, $d_{between}$ is given by:

$$d_{between} = \frac{d_1 - r}{2 \cdot N - 1} \tag{3.8}$$

and h_1 is given by :

$$h_1 = \sqrt{4 \cdot r^2 - (r + d_{between})^2} - r \tag{3.9}$$

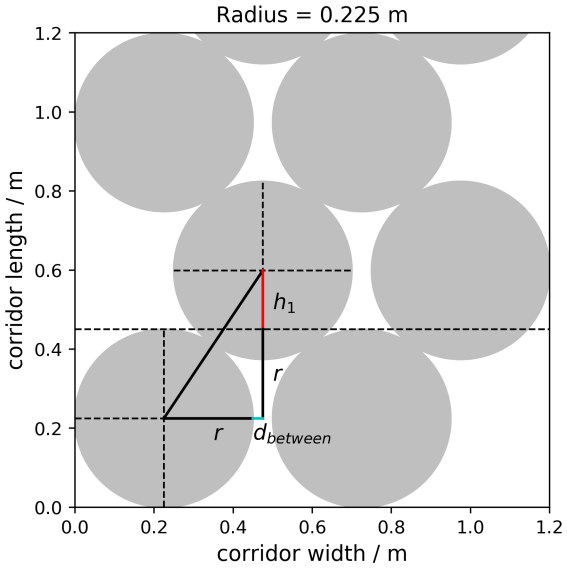

Figure 3.5: Reference lines and distances for configuration 1 (square) in order to calculate height h_1 if $d_1 > r$

The x-coordinates for uneven (see 3.10) and even rows (see 3.11) are then given by:

$$x_i = r + 2 \cdot i \cdot (r + d_{between}), i = 0 \dots N - 1 \tag{3.10}$$

$$x_i = r + (2 \cdot i - 1) \cdot (r + d_{between}), i = 1 \dots N \tag{3.11}$$

For configuration 2, uneven rows contain N circles and even rows N-1 circles as depicted in figure 3.6. The distance d_2 in x-direction between the circles in an uneven row is given by:

$$d_2 = \frac{w - 2 \cdot r \cdot N}{N - 1}$$

Thus, the height h_2 is given by:

$$h_2 = \sqrt{4 \cdot r^2 - (r + d_2/2)^2} - r \tag{3.12}$$

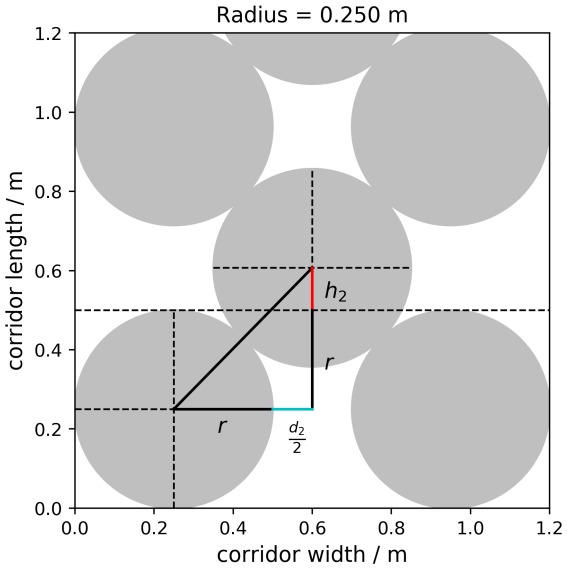

Figure 3.6: Reference lines and distances for configuration 2 (hexagonal) in order to calculate height h_2

The x-coordinates for uneven (see 3.13) and even rows (see 3.14) are then given by:

$$x_{i,uneven} = r + i \cdot (2 \cdot r + d_1), i = 0 \ldots N - 1 \tag{3.13}$$

$$x_{i,even} = \frac{x_{i,uneven} + x_{i+1,uneven}}{2}, i = 0 \ldots N - 2 \tag{3.14}$$

Having these configurations at hand, one can easily generate dense packings for any corridor width and circle radius r. To realise this, the circle coordinates and dimensions generated by the equations above are written into a file, which can be interpreted by *JPSreport* to determine the Voronoi density. An exemplary *JPSreport* inifile is given in the appendix A. The Voronoi density is read out in the measurement area for both configurations at widths 1.2 m to 5.6 m and varying circle diameter r with r = 0.15 m, 0.175 m, 0.20 m, 0.225 m and 0.25 m.

Figure 3.7 shows the resulting Voronoi densities in function of radius r for all widths. Differences in maximum Voronoi densities can be seen among both configurations, but

also within every configuration.

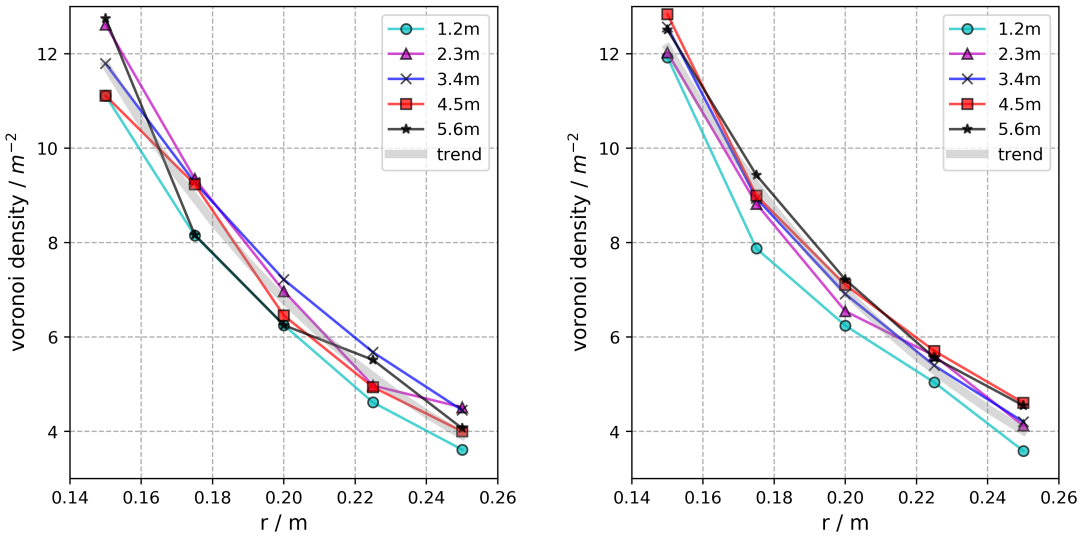

(a) Configuration 1 **(b)** Configuration 2

Figure 3.7: Maximum Voronoi densities of circles for both configurations and all widths with specific radius r. In general, the maximum Voronoi density increases with reducing radius r. Both configurations show differences in maximum Voronoi densities among each other, but also within every configuration for specific widths. A main observation is that the corridor width of 1.2 m shows lowest maximum Voronoi densities.

For configuration 1, the corridor of width w = 1.2 m shows the lowest densities. A density increase is always seen for the corridor width w = 2.3 m, depending on the radius r it is more pronounced. For width w = 3.4 m, the density sometimes increases or is equal to that of w = 2.3 m except for r = 0.150 m. As for the wider corridors, these show a different behaviour. They either result in equal maximum densities or are sometimes rather low and equal to those of corridor width w = 1.2 m. This might indicate that for a square packing, a density increase is only relevant in narrower corridors.

As for configuration 2, the narrowest corridor shows the lowest densities. Quite different to configuration 1, the hexagonal configuration most of the time shows a continuous density increase for a specific radius r over all widths. For both configurations, the narrowest corridor always results in significantly lower densities showing that some boundary effect exists. This is further illustrated in figure 3.8, where Voronoi cells look differently around walls. Especially in a narrow corridor, this boundary effect will have an effect during the measurement.

To further show this effect and its magnitude, a short demonstration is done by establishing the density difference between a squarish and a hexagonal Voronoi cell. It

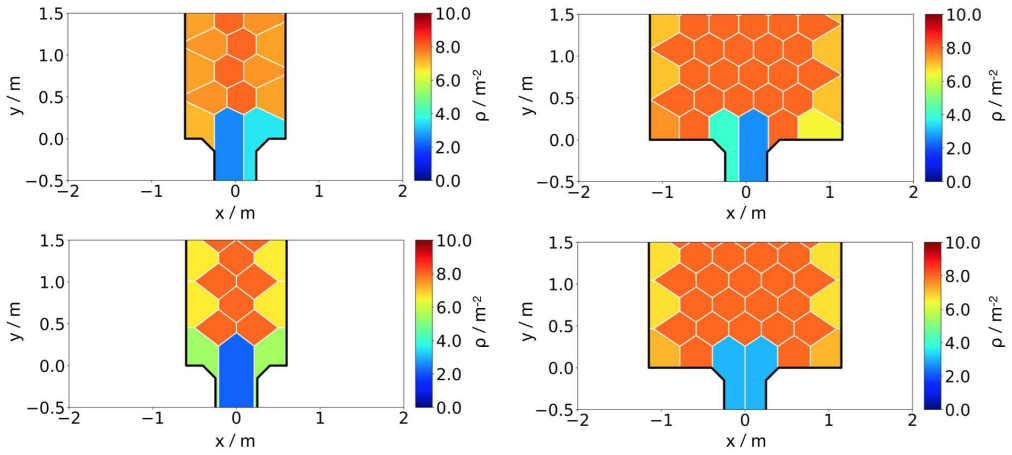

Figure 3.8: Boundary effect around walls for configuration 1 (above) and configuration 2 (below). Voronoi cells behave differently around the static walls. Especially in a narrow corridor, this boundary effect will have an effect in the measurement area.

is referred to appendix figure D.2 for figures. The density in a squarish Voronoi cell is given by:

$$\rho_{sqr} = \frac{1}{4r^2} \tag{3.15}$$

The density of a hexagonal Voronoi cell is given by:

$$\rho_{hex} = \frac{1}{2\sqrt{3} \cdot r^2} \tag{3.16}$$

The density difference between a square and hexagonal Voronoi cell is then approximately given by:

$$\Delta\rho = \frac{0.04}{r^2} \tag{3.17}$$

This difference is non-negligible regarding the $1/r^2$ dependency. It is also referred to the representation in the appendix figure D.3. However, there may be cases where Voronoi cells at walls appear in different forms such as triangles, which changes equation 3.15 and augments the density difference even more.

Furthermore, the relations found in figure 3.7 can be estimated by an exponential function in order to establish a width-radius-density relation. Thus, an estimation of the circle radius necessary in order to obtain maximum Voronoi densities is possible. The approximated mean functions are given in equation 3.18 for configuration 1 and 3.19 for configuration 2. Both functions have a correlation index of 0.986.

$$\rho(r) = 61 \cdot e^{-11 \cdot r} \tag{3.18}$$

$$\rho(r) = 64 \cdot e^{-11.1 \cdot r} \tag{3.19}$$

A further analysis is that of maximum possible neighbours. Figure 3.9 shows two analyses for a hexagonal configuration with circle radius r = 0.175 m. On the one hand, the agent network inside a corridor length of l = 2 m for all widths is determined. This network grows with the size of the corridor as can be seen in Figure 3.10. However, for the narrow corridor, this consideration results in a deviation from the linear relation found between the wider corridors.

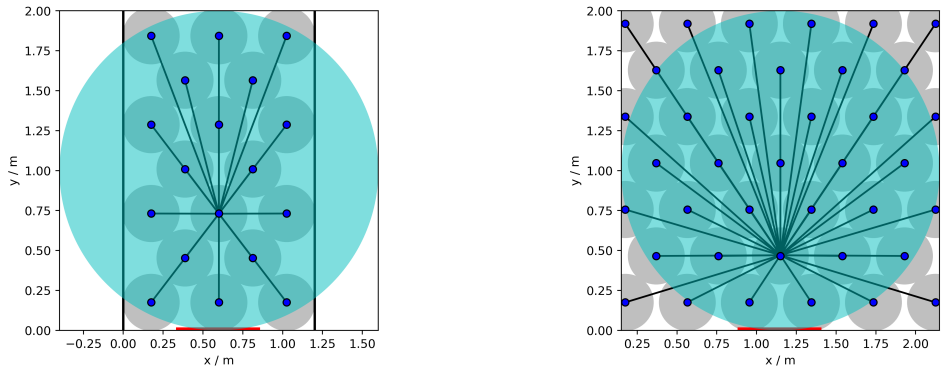

(a) w = 1.2 m **(b)** w = 2.3 m

Figure 3.9: Maximum possible neighbours for a hexagonal configuration in a given area is lower in a narrow corridor as the number of agents only augments vertically, whereas in a wide corridor it augments both vertically and horizontally. Moreover, the circles can pack denser in a wider corridor.

On the other hand, an approach was used to determine immediate neighbours, which is done within a circle area of r = 1 m. This aims at considering effects more locally right before the exit. Here, a convergence to a maximum number of immediate neighbours of about 28 circles can be seen, the narrow corridor resulting in 15 immediate neighbours. This is due to the fact, that the number of agents in a narrow corridor can only increase vertically, whereas in the wide corridor the arrangement can take place in both directions as a vertical and horizontal augmentation. Furthermore, the hexagonal configuration itself can better fill the interspaces in larger corridor widths, which augments the packing of circles inside the circle area somewhat too.

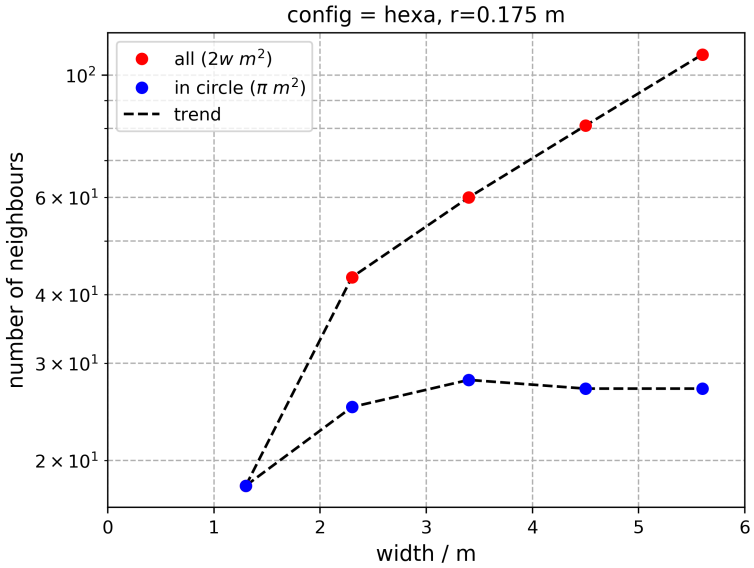

Figure 3.10: Reduced maximum number of neighbours in narrow corridor, in this case for r = 0.175 m. Both the whole corridor area (15 immediate neighbours in narrow corridor) and a circle area of r = 1 m show this behaviour, a convergence to 28 circles obviously been seen in the constant circle examination for wider corridors

3.3 Preparation of initial conditions

This section focuses on the initial agent distribution and the generation of comparable initial densities. This is necessary as this initial condition as influencing parameter cannot be ruled out. In order to obtain stability of simulation results, a reasonable number of replicated runs with respect to the initial densities needs to be made. The RiMEA guideline [29] states that without a specific analysis, a number of 10 runs should be carried out to "allow a statistically sound statement".

The trajectory calculation is done with *JPScore* for which a full exemplary initial configuration file is given in the appendix A. As the experimental data holds best empirically for a number of participants of around 50, the simulations are done with N=50. Furthermore, N is in a comparable range so that experimental and simulation curves can be put side by side. Nevertheless, simulations with N=25 and N=75 will be kept out to analyse the simulation behaviour. However, it should be noted that there is scarce experimental data to compare it to.

The initial Voronoi densities in the experiment are roughly identical and can be found between 2-4 m^{-2}. The respective values are summed in Table 3.3, the median is given by 2.8 m^{-2}. This initial condition should be met in the simulation as well. Therefore, the following calculations are made for a specific number of agents N and

Table 3.3: Initial Voronoi densities for selected experimental runs

run	050	060	110	120	150	160	230	240	250	260	270	280
ρ	2.5	2.5	3.3	4.2	2.1	2.7	2.1	2.4	3.2	2.8	3.5	3.0

desired initial density $\rho_{initial}$ relative to the whole corridor area. The number of agents N that can be distributed inside a corridor of width w and length l with a desired initial density $\rho_{initial}$ is then given by:

$$N_{cor} = \rho_{initial} \cdot w_{cor} \cdot l_{cor} \tag{3.20}$$

Now, two cases need to be distinguished. In the first case $N_{cor} \leq N$, meaning that not all agents fit inside the corridor, so that the number of agents to be distributed outside the corridor area N_{out} is calculated by:

$$N_{out} = N - N_{cor} \tag{3.21}$$

However, for the second case $N_{cor} \geq N$ more than N agents fit inside the corridor. As the distribution is wanted for a specific number of agents N, a reduced length of the corridor l_{red} needs to be calculated:

$$l_{red} = \frac{N}{w_{cor} \cdot \rho_{initial}} \tag{3.22}$$

It should be noted that $\rho_{initial}$ is calculated with respect to the whole corridor area and not via the measurement area. The effective Voronoi density can only be measured afterwards. Furthermore, N_{cor} is rounded and the subsequent calculations done with that rounded value. If the first case comes into effect, the geometry thus needs to be extended accordingly. The distribution area of number of agents N_{cor} is limited to $y_{min} = 0$ and $y_{max} = l_{cor}$. Table 3.4 gives exemplary calculated values for $\rho_{initial}$= 2.5 and N = 50.

width (m)	1.2	2.3	3.4	4.5	5.6
$\boldsymbol{N_{cor}}$	20	39	50	50	50
$\boldsymbol{N_{out}}$	30	11	0	0	0
$\boldsymbol{l_{red}}$	/	/	5.9	4.4	3.6

Table 3.4: Calculated values N_{cor}, N_{out} and l_{red} for 50 agents

In order to get a more homogeneous distribution within the corridor, several layers

with groups are defined. This is further illustrated by figure 3.11, where the initial distribution for one seed is displayed.

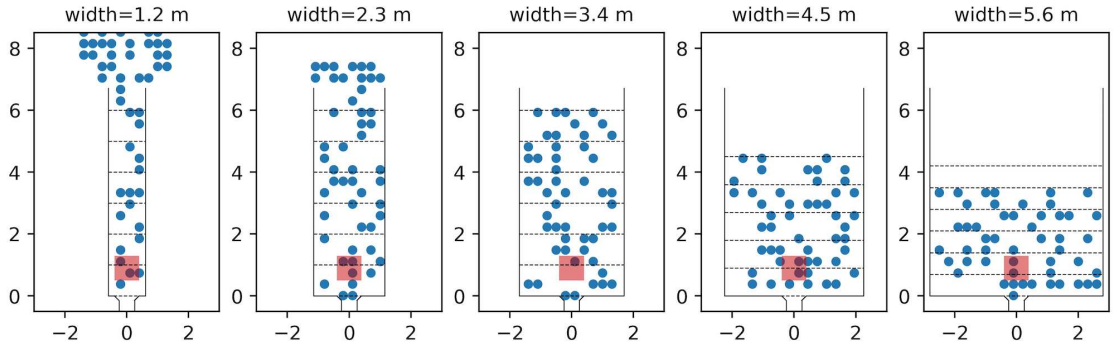

Figure 3.11: Snapshots of initial distributions. Agents are represented by blue dots, layers indicated by dashed lines and the density measurement area drawn in red.

The number of agents N_{out} is distributed with the condition $y_{min} = l_{cor}$ without layering. In the second case, the maximum distribution area for N is simply limited by $y_{min} = 0$ and $y_{max} = l_{red}$. Again to make the distribution in the corridor more homogeneous, different layers with groups are defined.

From figure 3.12, it can be seen in the upper bar plot that the individual initial Voronoi density in the simulation differs from the targeted $\rho_{initial}$= 2.5. The lower and upper boundaries of the experimental values are given by 2.1 m^{-2} and 4.2 m^{-2}, which equivalents to a maximum comparable difference of 16% downwards and 100% upwards. The exceeding relative differences are thus coloured red. This shows that the generated approach is just a work-around in order to fulfil the initial density requirement and should not be understood as producing robust initial conditions, which would need further development.

However, it is possible to take a look at the convergence of mean or strong convergence of the generated initial Voronoi densities per width. The strong convergence X_n of n independent runs for the quantity ρ_i is given by:

$$X_n = \frac{1}{n} \sum_{i=1}^{n} \rho_i \tag{3.23}$$

The lower plot in figure 3.12 shows X_n for different number of runs up to 10 runs for all widths. When simulating enough runs, the mean initial Voronoi density will converge. This can be explained by the law of large numbers [30]. In this case, it always converges to a density $\rho \in [2, 4]$, which is rather near to the mean experimental Voronoi density of 2.8 m^{-2}. Thus stable long-term results of random input values are guaranteed, which

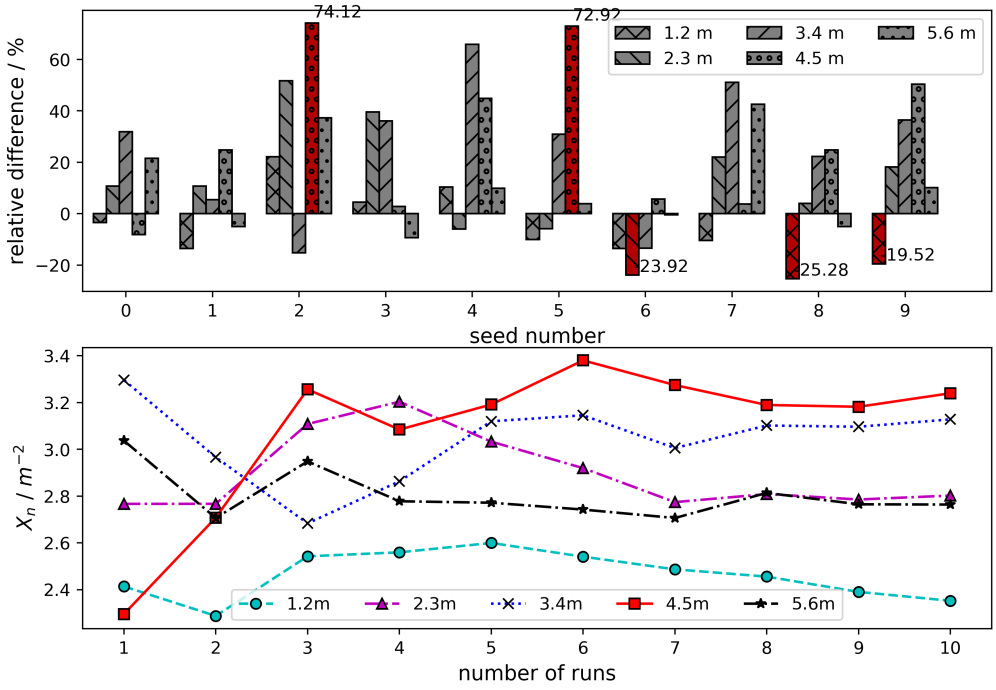

Figure 3.12: Top: scattering in initial Voronoi densities for all widths. Bottom: strong convergence of Voronoi density mean for 10 runs for all widths showing that stable long-term results of random input values are guaranteed, which verifies the sufficiency of this approach for modelling comparable initial densities

verifies the sufficiency of this approach for modelling comparable initial densities. These calculations are done equally for N = 25 and N = 75 in order to guarantee comparable initial densities and can be found in appendix D.1.

3.4 Model parameters

This section addresses the determination of agent parameters, namely the desired speed v_0 and agent diameter size l. The pedestrian flow inside the simulation is adjusted via v_0 as proposed in [31], the agent diameter size l determined such that maximum densities observed in the experiment are feasible in the simulation. Calibration parameters are altered to model high density states and further agent parameters such as time gap parameter T repurposed as motivational parameter in the given model. Additionally, the modelling of two types of agents is dealt with.

3.4.1 Physical agent parameters

The mean outgoing flow for all runs in the experiment is around 1.1 s^{-1}. This flow rate is tuned in the simulation via v_0 so that comparability is better achieved. The analysis with the standard parameter set (l= 0.3, T=1.0, a=5.0, D=0.1) shows that v_0 = 1.2 m/s gives best accordance. This is further illustrated by figure 3.13 which displays N-t curves for all 5 widths for specific desired speeds v_0.

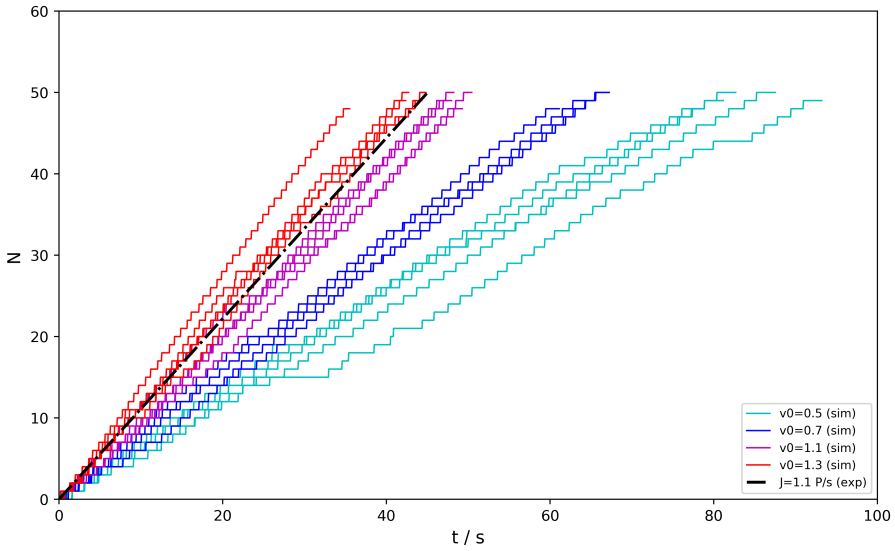

Figure 3.13: N-t curves for all widths for different desired velocities v_0 compared to mean experimental flow depicted in black

The agent size l influences the maximum density possible. Therefore, the maximum experimental density is taken into account to determine the standard agent size l for the simulation. Calculating with the transformed equation 3.24 from equation 3.19 for a maximum experimental density of 9 m^{-2}, which is the contracted stage at maximum, r = 0.175 m is obtained.

$$r(\rho) = -\frac{ln(\rho/64)}{11.1} \tag{3.24}$$

This is used as standard agent parameter size l, so that agents have a diameter of 0.35 m. The pedestrian size l is a crucial parameter as it defines the maximum density reached. It should be noted that this is of course a rather small shoulder width, literature [32] giving an approx. adult shoulder width of l = 0.46 m. However, the area resulting from this circle is about 0.096 m^2. As pedestrians are better described with ellipses, this area transfers into an ellipse with semi-axes a=0.23 m and b=0.13 m, which is a

justifiable agent size. This makes the circle analogy comparable. Furthermore, even when leaving this analogy as non-conclusive, the circle diameter of 0.35 m could be seen as a contracted pedestrian.

As for the time gap parameter T, this is adjusted by default at T = 1 s as this gives good correlation with the fundamental diagram, which is derived from empirical measurements. However, this parameter could be of use for motivation representation. Therefore it will be varied as well and discussed in the following section.

3.4.2 Reproduction of motivation

In this section, general thoughts are made regarding the representation of motivation inside the model. It should be noted that until now the model contains no explicit implementation for quantifying motivation. Possible working points are the direction model and the optimal velocity function.

On the one hand, the direction model offers two calibration parameters: the repulsion rate a and the repulsion distance D. The standard calibration is adjusted by default with a = 5.0 and D = 0.1. The idea is to change these calibration parameters and use them to reproduce low and high motivation conditions without them being motivational parameters in the first place. Exemplary repulsion functions are shown in figure 3.14.

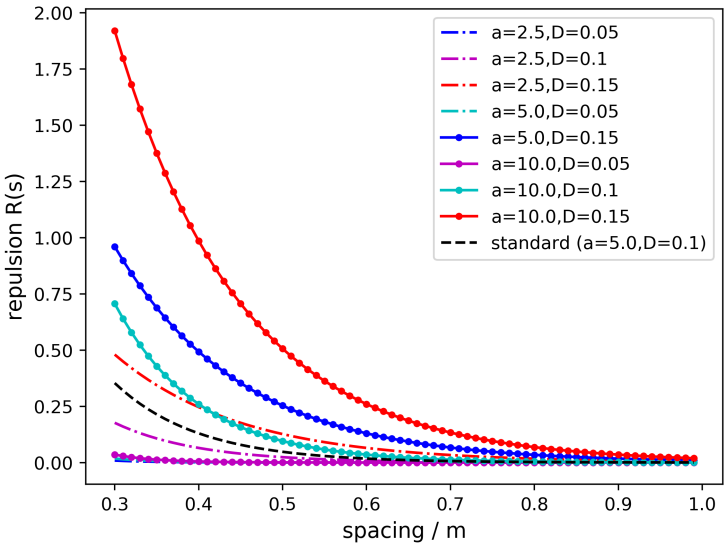

Figure 3.14: Representation of repulsion functions for altering repulsion rate a and distance D in the operational model

The repulsion rate a in the model actually represents the influence from other agents on an agent's individual moving direction. Applying this to the real world, this

parameter a has no meaning as it is a variable used for calibration purposes. However, it could be interpreted as a behaviour of considering neighbours and taking neighbours into account or not when deciding about the moving direction. Thus, it could be used as one way of representing motivation in the model with the following approach: highly motivated agents don't take other neighbours into account when calculating their moving direction, whereas low motivated agents want to cooperate and thus change and adapt their moving direction. Therefore, it is expected that higher values of parameter a will result in gap filling whereas lower values will cluster the agents. As for the repulsion distance D, this parameter gives the range of parameter a.

With these assumptions, the calibration parameters a and D are varied through a number of simulation runs for different widths. As for the sampling of these parameters during the variation, a random sample would be very inefficient to test all necessary combinations. Therefore, an orthogonal Latin hypercube (OLH) sampling [33] with a specific design region of $\Delta a = 3.0$ and $\Delta D = 0.06$ is used to reduce the necessary simulations without a validity trade-off. This is shown in figure 3.15.

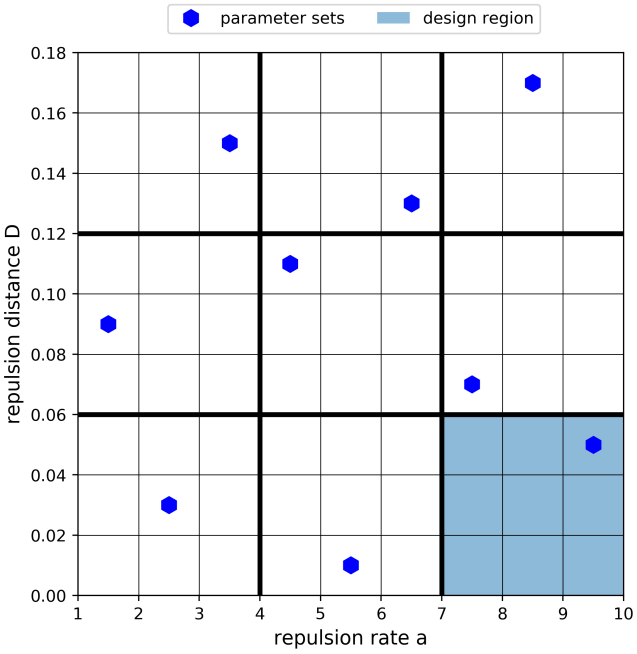

Figure 3.15: Orthogonal Latin hypercube sampling for repulsion rate a and repulsion distance D, the blue square representing the design region and a blue hexagon the specific parameter set

The OLH approach offers the benefits of an ordinary Latin hypercube by considering the samples already calculated, but also guarantees for a uniform scattering, more precisely density, in all design regions. The emerging dynamics from these variations

can be found in the results section.

On the other hand, the optimal velocity function offers a second approach to further model a high motivation state. The latter function uses s, l, v_0 and T as input parameters. The pedestrian size l and v_0 are fixed by the analyses above. The minimal spacing s is calculated configuration-dependent. However, a variation of the time gap parameter T is possible. Changing the time gap parameter T will result in different piecewise linear velocity functions. Some example functions for T = 1.0, T = 0.5, T = 0.25 and T = 0.1 are shown in figure 3.16.

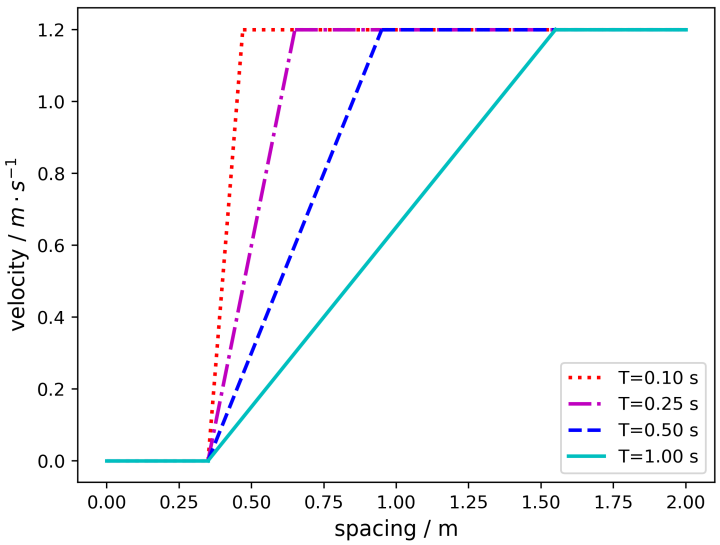

Figure 3.16: Representation of velocity functions for altering time gap parameter T in the operational model

By reducing this parameter, the agents velocity can be increased even when the spacing is low up to the point where:

$$\lim_{T \to 0} V(s) = v_0 \tag{3.25}$$

This would make the speed a driving parameter for motivation in this model and ultimately result in a fast contracting stage. Furthermore, the time gap T actually has a real-world meaning in that it represents the urge to move up when there is free space.

However, it should be noted that both approaches to reach a high motivation state in the simulation shown here do not model the phenomena of pushing.

3.4.3 Defining different types of agents

The experiments show two types of people. Therefore, an approach to represent and analyse this circumstance is taken by defining two populations, which are in fact two different operational models in action. This is done with respect to different parameters a and T, the repulsion distance D being the same for everyone. A simple modulo condition is checked on the specific agent's identifier in both the direction and velocity model to split the agents into two populations. To be able to differentiate the two populations, the highly motivated population is highlighted with an available spotlight color mode offered by *JPScore*.

Code snippets in appendix B show an exemplary implementation for time gap parameter sets T = 0.25 and T = 1.0 as well as repulsion rate parameter sets a = 2.5 and a = 5.0 with D = 0.05.

3.5 Further configuration setups and automation

Concerning the route choice algorithm, two approaches are possible: a navigation graph, which builds a permanent routing network by using the Dijkstra algorithm or a floorfield, which uses the Floyd-Warshall algorithm to build individual floorfields. The advantage of the latter is the non-necessity for convex rooms. However, it should be noted that the floorfield router gives intermediate targets. Simulations will be done with both approaches to calculate the shortest path and valid desired directions. Furthermore, the maximum simulation time is set to 200 s and seeds will be automatically varied.

Concerning the measurement of density and flow, *JPSreport* is used. The area for measuring the Voronoi density is given by a square built with x_{min} = -0.4 m, x_{max} = 0.4 m, y_{min} = 0.5 m and y_{max} = 1.3 m. The measuring line for the outgoing flow at the exit is given by x_{min} = -0.25 m, x_{max} = 0.25 m at y = 0 m. A full exemplary inifile is given in the appendix A.

The simulation variations concern 3 model parameters, the number of agents and different types of agents. This will result in a number of simulations, so that automation is a key component of this thesis. Therefore, several bash and python scripts are written to facilitate the automatic trajectory calculation and data readout. A list of all written bash and python scripts can be found in appendix E.

Generally, the work flow begins with a master initial configuration file, which is manually created and used as a basis for all simulations. For a given set of parameters, a master bash script will produce the desired number of directories with the necessary initial configuration files, adapt the seeds and update the parameters. A second bash

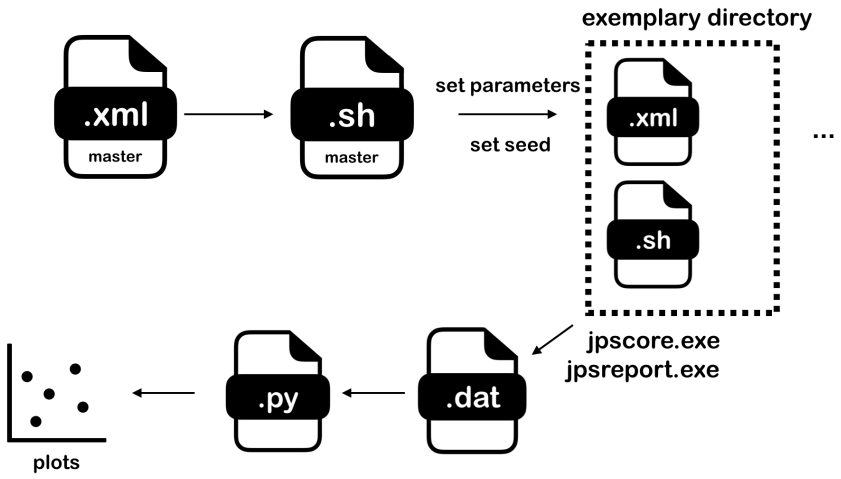

Figure 3.17: General automated work flow beginning with a master initial configuration file and a master bash script producing specific simulation directories. A second bash script will execute the simulations for all seeds and widths using *JPScore*. *JPSreport* then produces analysis data which is plotted using various python scripts.

script inside every directory will execute *JPScore* to calculate the trajectories and *JPSreport* to analyse them. An automated flow check is done as well. A python script will then read out the produced data. Further plotting scripts will produce Voronoi diagrams, time-density series, width-density relations in a specific time interval, cumulated trajectories and individual distance and time to target plots.

Chapter 4

Results and analysis

4.1 Variation of corridor width

This section presents the simulation results for the corridor width variation according to the five specific experimental widths.

4.1.1 Voronoi densities

A first glance at Voronoi diagrams in figure 4.1 for all corridor widths at t = 5 s shows that the density in front of the bottleneck gradually increases, the density for a corridor width of 1.2 m being significantly lower in comparison to a corridor width of 5.6 m. Thus, a general density increase in front of the bottleneck with the enlargement of corridor width can be observed in the simulation. Two important observations can be made: individual Voronoi cells reduce the most between corridor width w = 1.2 m and w= 2.3 m and the wall influence diminishes from width w = 3.4 m onwards.

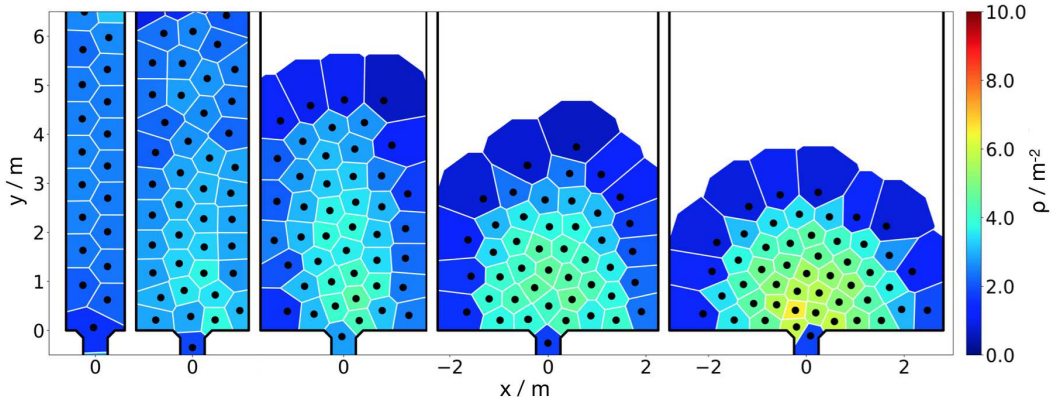

Figure 4.1: Voronoi plots for t = 5 s for all widths indicating a continuous density increase, the main increase being situated between w = 1.2 m and w= 2.3 m

However, one can note as well that the density increase for the widest corridor is distributed uniformly in a circular shape and that agents further away from the exit actually show Voronoi cells of the same magnitude found in the more narrow corridors. This indicates a model behaviour that may be independent from the width variation and is further discussed in section 4.2.

To extent these snapshot results, the specific Voronoi density in front of the bottleneck inside the measurement area for a time window $\Delta t = 5s$ reaching from t = 5 s to t = 10 s is read out. From this, an individual mean value can be calculated. The simulation results for every width are backed up with 10 calculated seeds, so that all in all 50 simulations make up the width-density analysis. When analysing all data points, an overall scattering in density for different seeds but the same width is observed. This is related to small differences in the initial densities and thus slightly different density trends. Thus, a general mean for every width is calculated. These mean values are then interpolated by an exponential function. The resulting curve is shown in figure 4.2 together with both curves resulting from the experimental data. The exponential best fit is given by $5.48 \cdot (1 - e^{-0.45 \cdot x})$.

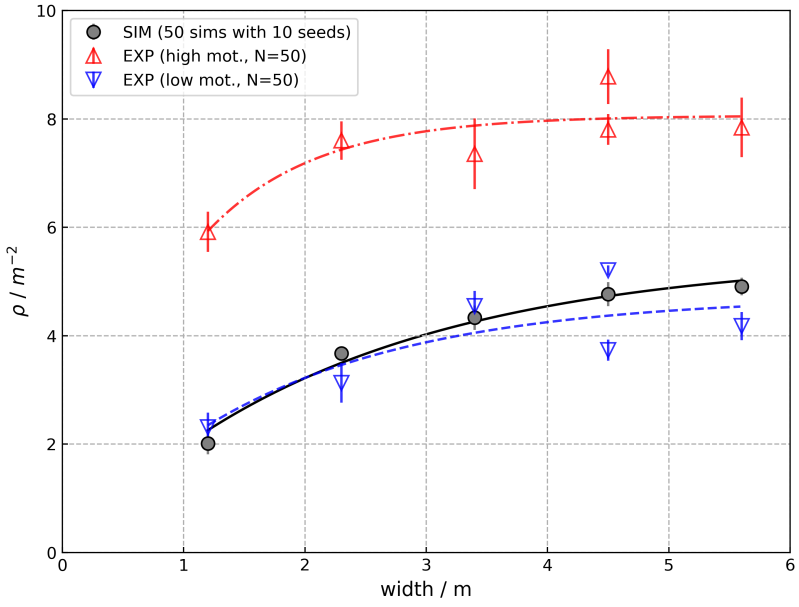

Figure 4.2: Condensed width vs. density plot. The dark blue and red lines represent the experimental data for low and high motivation, whereas the grey line is the simulation outcome with N=50, a=5.0, D=0.10, l=0.35, v_0=1.2 and T=1.0

In general, the generated simulation curve for the width-density relation is similar to the experimental curve of low motivation. At first, this makes sense and could be

expected as the model does not account for any motivational parameter in this stage. In addition, this width-density relation better illustrates the fact that the density increase is rather significant at the beginning, nearly $\Delta\rho \approx 2\ m^{-2}$ for a width transfer from w = 1.2 m to 2.3 m in comparison to $\Delta\rho \approx 1\ m^{-2}$ for a width transfer from w = 2.3 m to 5.6 m.

Furthermore, a look at the time density series in figure 4.3 gives a greater insight into the evolution of the density in front of the bottleneck for all widths. Here, series for 3 seeds for every width are represented.

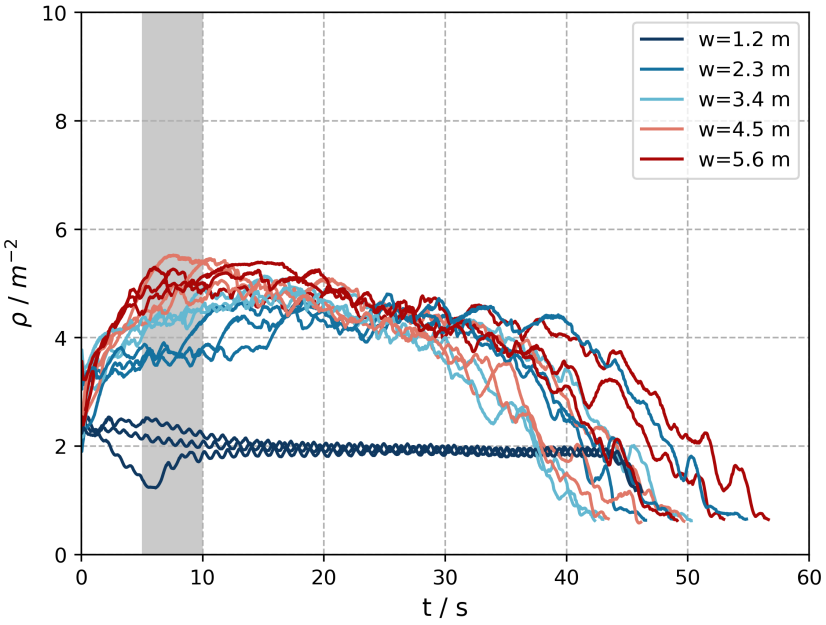

Figure 4.3: Simulated time-density series for 3 seeds and 5 widths with standard calibration parameters and customized agent parameters

It can be seen that for a width of 1.2 m, the density drops to about 2 m^{-2} just like in the experiment. The trend for this width also shows an oscillating nature, which indicates a repeating and stationary state. This does not happen for all remaining widths. For a width of 2.3 m, the resulting density in the measurement interval is nearly twice as high, but always lower than the densities for the three remaining widths. The time density series for width of 3.4 m is centered between those of 2.3 m and the two remaining widths, 4.5 and 5.6 m. The latter give the highest densities, but vary and superimpose. All together, the time-density series of the three highest widths are again rather similar.

Moreover, the simulation curves show less noise than those from the experiment and intermediate peaks do not arise. The run durations are situated between 40 s up to

about one minute. Obviously, these run times are rather similar in the simulation due to the constant number of 50 agents.

4.1.2 Trajectory analysis

To get an overview of the overall dynamics, condensed trajectory plots are generated for all corridor widths as shown in figure 4.4. All trajectories are plotted with low alpha values to facilitate the emergence of spatio-temporal patterns.

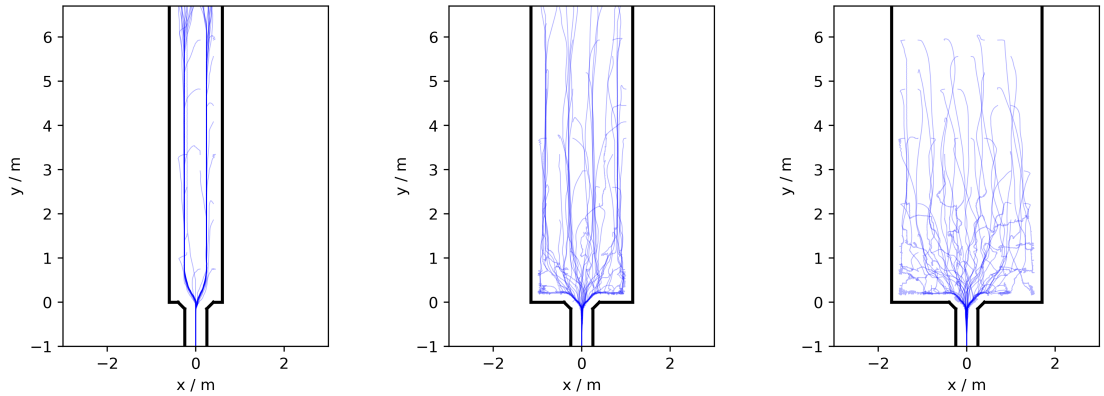

(a) 2 stable lanes, cut at exit

(b) 4 stable lanes, small cluster

(c) lanes dissolving more into cluster

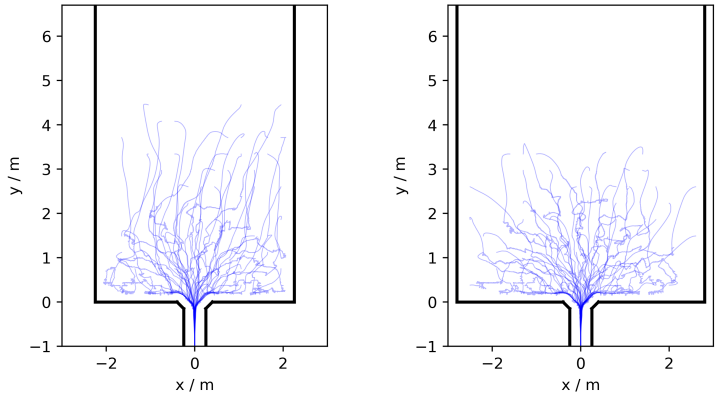

(d) cluster further evolving

(e) full cluster

Figure 4.4: Spatio-temporal patterns for all widths from condensed low alpha trajectories

As for the narrowest corridor, the condensed trajectories result in the formation of two stable, equally opaque queues. This indicates that these both lanes have an identical degree of capacity utilisation. Both queues intercept right before the exit. The trajectories for width w = 2.3 m emerge to 4 lanes at the beginning and intercept earlier.

A significant fraction of trajectories cut in from both sides right before the exit. For larger widths, this observed lane formation is continuously dissolved and trajectories intersection happens even earlier. This results in a sort of clustering.

The essential transition from a lane configuration into a cluster-like structure already happens between w = 1.2 m and 2.3 m. To illustrate this transfer more clearly, figure 4.5 shows all trajectories together in one plot. The doubling of the corridor width makes the appearance of at least four more routes possible. In wider corridors, these side routes persist and new routes emerge between those routes established in the corridor width before.

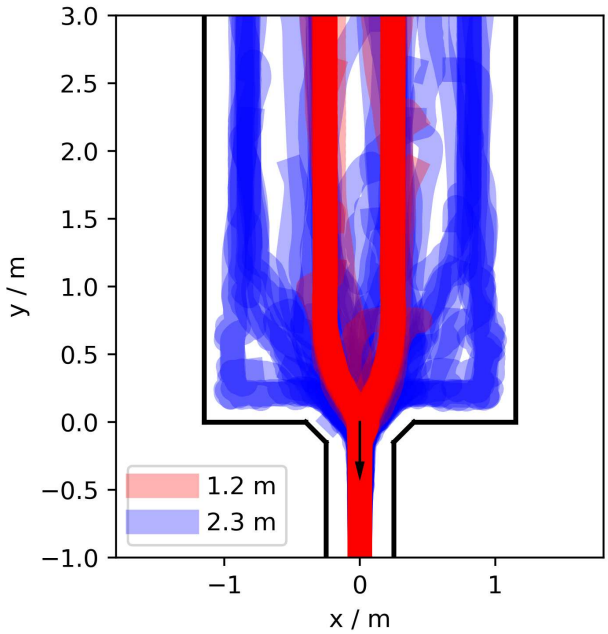

Figure 4.5: Condensed trajectories for width 1.2 m in red and for width 2.3 m in blue. 2 lanes meet in the narrow corridor, whereas at least 6 have to meet in the 2.3 m wide corridor

The reason for these different configurations appearing is not dismissed lightly as it is not straightforward. Both the modelling environment and the real world show lane formations in narrow corridors and clustering in wide corridors, which reveals an inherently physical character. In the following, the simulation conditions and the operational model for different widths are further analysed to get a better understanding of this phenomena through simulation analysis.

4.1.3 Initial desired directions

First, a look at initial conditions is taken before any movement occurs. The desired moving direction, represented in the simulation by e_0, is either given by the middle point or the nearest point of a segment line that needs to be crossed by an agent. In the narrowest corridor, the desired moving direction is rather the same for everyone as can be seen in figure 4.6a, which makes concurring aspects small. Therefore, the probability of interaction and thus the probability of collision is low. In the widest corridor, the desired moving directions are different as is seen in figure 4.6b and concurring aspects are high, which means that the probability of interaction and the probability of collision is high. To further strengthen this, one could calculate the divergence of both unit vector fields. In the narrowest corridor, this divergence would evaluate to zero, but would be non-zero and positive in the widest corridor.

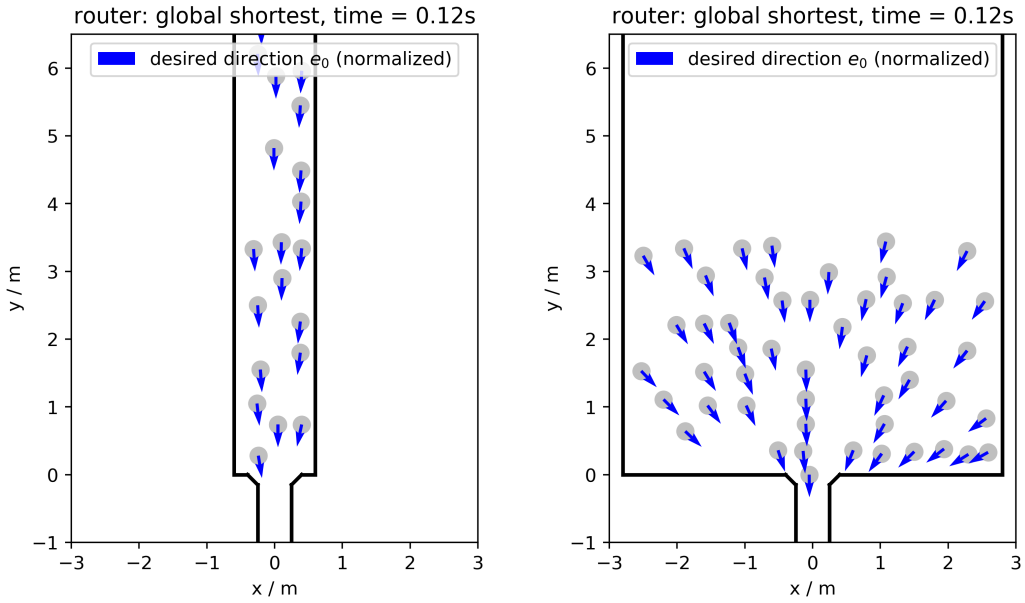

(a) width w = 1.2 m **(b)** width w = 5.6 m

Figure 4.6: Representation of desired direction e_0 at t= 0.12 s using global shortest router without floorfield

A much more interesting analysis is however the consideration of changes in x-components of desired directions for all agents. For this, use of box plots is made. These can represent the minimum and maximum, first and third quartile, mean and median of a given data-set in a very consolidated format. Figure 4.7 shows these box plots for 4 different runs and all widths. As for the narrowest corridor, the x-components of the desired directions are mainly situated around 0.1 vector units, maximum values of 0.2

being possible due to being near to the exit. From then on, the following corridor widths show a successive augmentation of the mean and median x-component. Furthermore, the domain is extended continuously and the box plot, containing 50% of the respective data, grows accordingly. This analysis shows the actual divergence in vector directions obtained when augmenting corridor width.

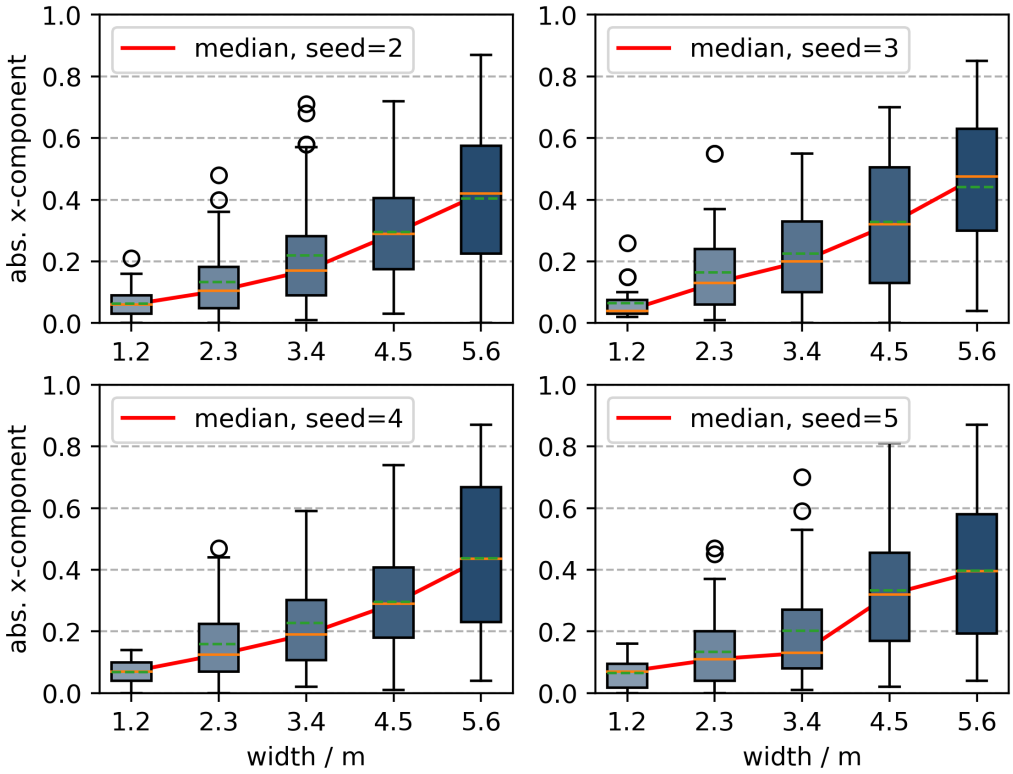

Figure 4.7: Boxplots of absolute x-components per width for four different seeds showing minimum and maximum, first and third quartile, mean (dashed green line) and median (orange line) of a given data-set, dots represent outliers. The quantity of agents possessing pronounced x-components increases with width w. A red line additionally links the medians to show the increase, which is a different course per width depending on the seed-dependent initial distribution

As a side remark, it makes a difference for this initial stage analysis as to which router is used. Looking at the e_0 directions when using the floor field router, different desired directions result. This is due to the intermediate calculation of targets. The relevant plots are shown in the appendix figure D.1.

4.1.4 Moving directions

Coming from this stationary observation, the movement stage is analysed. For a given time step, the simulation determines the desired direction e_0 and the repulsion term, which will give the moving direction e_i. The repulsion term is dependent on the repulsion rate a, repulsion range D, pedestrian size l and the individual distance between the agents s_{ij}. From these parameters, only s_{ij} can be different in the two configurations as the other parameters are left constant. However, the specific repulsion is calculated for every pedestrian and so the repulsion term is a sum parameter. Due to the boundary condition difference of maximum possible neighbours made clear in section 3, this term will always be bigger for wide corridors, even when at maximum densities.

As this s_{ij} is reduced from the pedestrian size l, the term inside the exponential function and thus the R_{ij} term will be high when s_{ij} is small. Thus, taking a look at both corridor configurations, the number of small s_{ij} is low in the narrow corridor and high in the wide corridor. Therefore the repulsion sum will be high in the wide corridor and rather low in the small corridor. Indeed, when reading out the values of this sum term, it can be seen in figure 4.8 that for w = 1.2 m, these factors are rather low whereas high factors are reached in the wide corridor with w = 5.6 m.

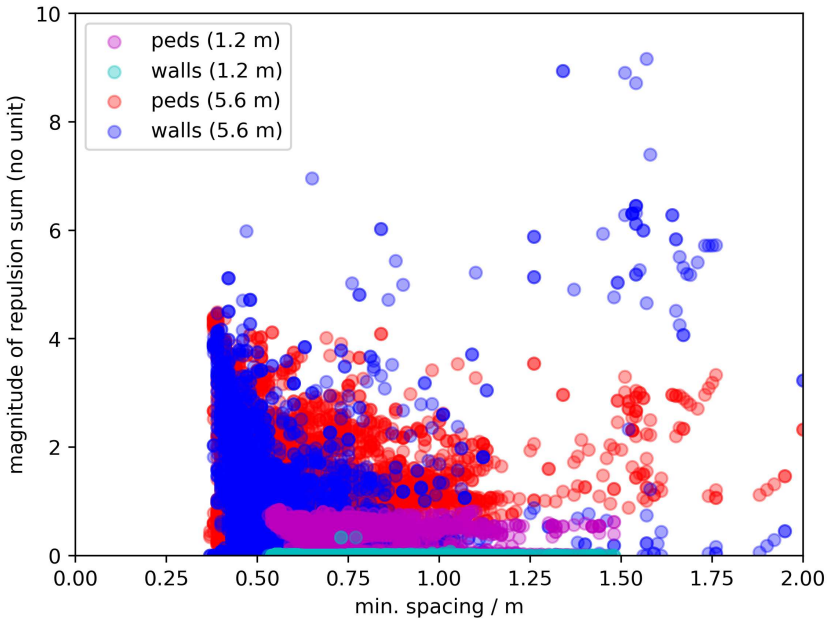

Figure 4.8: Magnitude of repulsion sum for narrow and wide corridor for stationary state (after t = 2 s)

Therefore, e_i in small corridors will only differ a little from e_0. In wide corridors, e_i

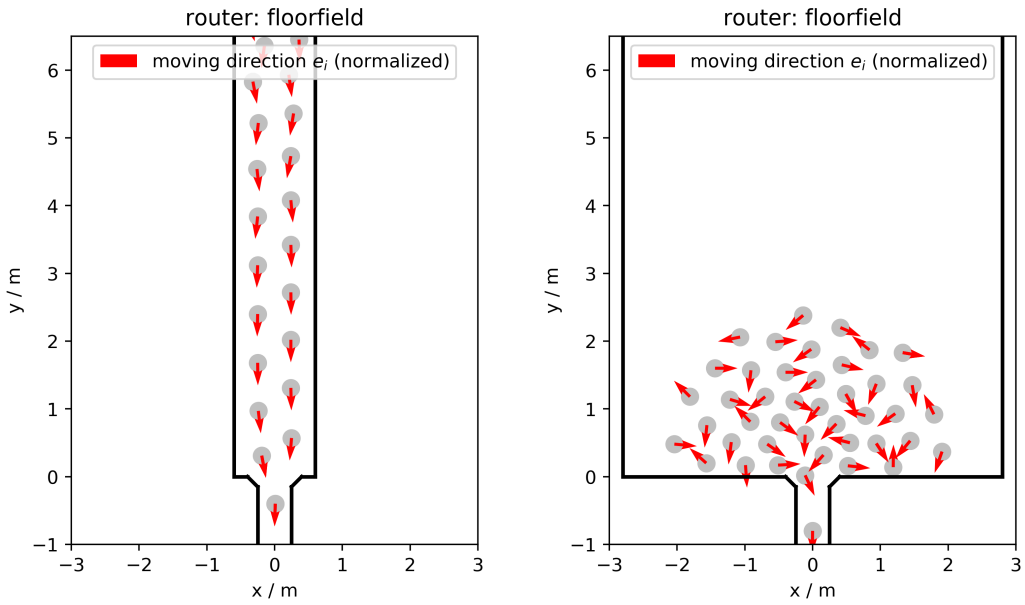

(a) width w = 1.2 m **(b)** width w = 5.6 m

Figure 4.9: Moving direction e_i in the simulation for narrow and wide corridor

will be significantly different from e_0. This is shown qualitatively in figure 4.9. Further plots in the appendix figure D.4 accompany this. As a consequence, agents will have to make significant adaptations when starting to move in wider corridors, whereas agents in the narrowest corridor only need to adapt a little when starting to move. This ultimately favours a lane arrangement for the narrowest corridor from this initial condition, however opens up the possibility for overtaking and space filling in the more wider corridors.

4.1.5 Possibility of space filling and overtaking

Furthermore, due to the different arrangement of walls in a narrow and wide corridor, the overtaking and space filling possibility will augment when widening a corridor. These possibilities will be used by the agents as already shown in the trajectory analysis. As this possibility is however non-existent in the narrowest corridor, solid queues, whose gaps can be no more filled, develop. Figure 4.10 shows snapshots at different times for the widest corridor. Here, 10 agents are situated in an area delimited by x_{min} = -0.6 m and x_{max} = 0.6 m, thus possessing an e_0 parallel to the side walls and are coloured blue. The other agents around them, 20 on every side, are coloured grey. At t = 0 s, the blue agents are starting to build up a two-agent-wide lane with spaces. At t= 3 s, first infiltrations from grey agents happen. The width of the lane is reduced from 2

agents to 1 agent respectively grey agents will take spots between the blue agents. This circumstance of being able to zip in is exclusive to the wider corridors and will make the interspaces disappear.

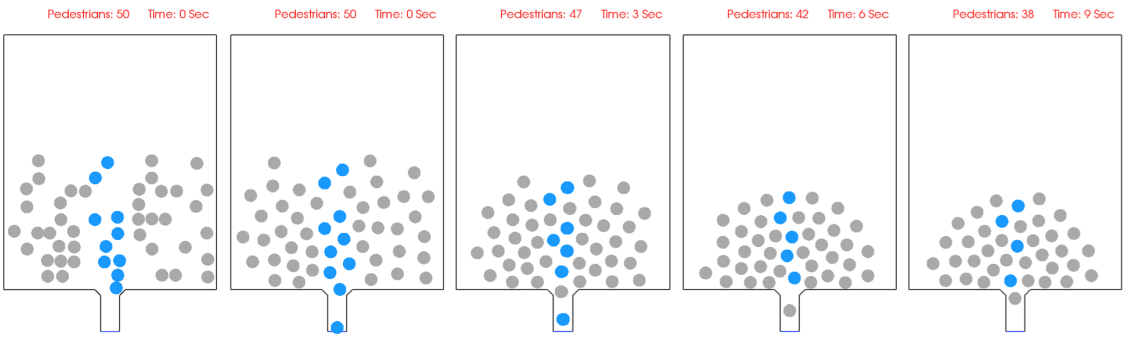

Figure 4.10: Snapshots at different times for a corridor width w = 5.6 m showing space filling

Furthermore, evaluating distance to target vs. time to target plots from the simulation shown in figure 4.11, the courses of the widest corridor show overtaking and cutting in line processes as there are agents nearer to the target that need longer than agents further away from the target. For the narrow corridor, a linear relation between distance and time to target is found indicating no filling or overtaking processes. The curves for an intermediate corridor width of 2.3 m merges both behaviours.

This also means that the minimal spacing s used for the velocity calculation is highest in the narrowest corridor. As the optimal velocity function uses v_0, s, l and T as input parameter, from which only s varies, higher velocities will be reached for narrow corridors.

Therefore, much steeper curves in figure 4.11 are observed for the widest corridor meaning that within a defined period of time there is no big reduction of the distance to the target. Thus the steepness of these curves represents the velocity in an inverse relation: the steeper the curve, the lower the velocity. This is also in accordance with the fundamental diagram, which reports that lower velocities will result in denser states.

Comparing these plots in figure 4.11 to the experimental ones, the accordance is good for the narrowest corridor with the exception of not having the waiting behaviour, which is not modelled. For the widest corridor, a significant steeper curve is seen and the free speed movement behaviour is absent because the initial distances are lower than in the experiment due to guaranteeing comparable initial densities. In addition, the curves for the widest corridor are bended like the experimental ones from high motivation which shows that the model approach indeed already shows a behaviour that was not intended to be modelled. It is again referred to section 4.2.

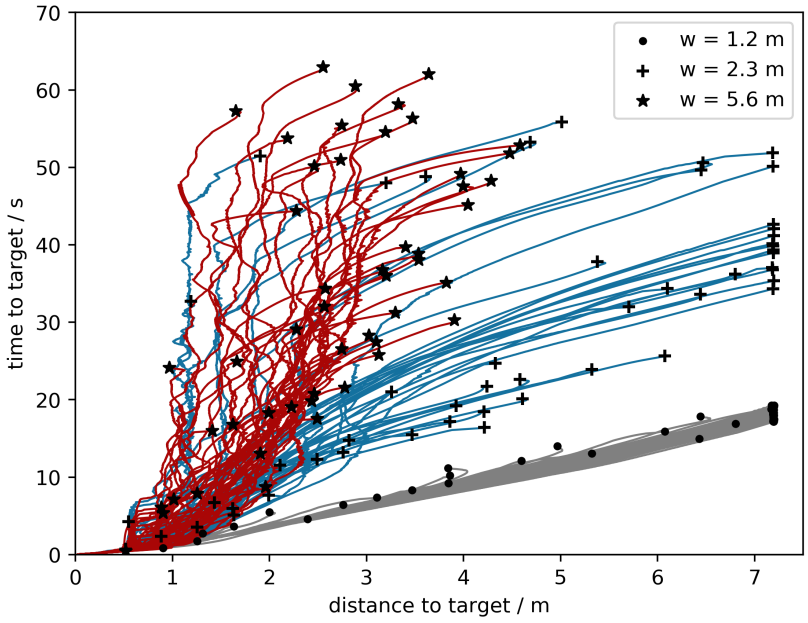

Figure 4.11: Time vs. distance to target plots showing overtaking

4.1.6 Blockage occurrence

A further and last observation made is that of blocking occurrence. A blocking stage is defined as a time interval $\Delta t \geq 2s$ in which no agent passes the exit. In the narrowest corridor, no blocking is observed. For the 2.3 m wide corridor, short blocking stages occur. For the widest corridor, some blocking stages double or even triple in duration. This is shown in figure 4.12. This observation needs to be considered and is further analysed in the following section as it is also linked to the number of agents.

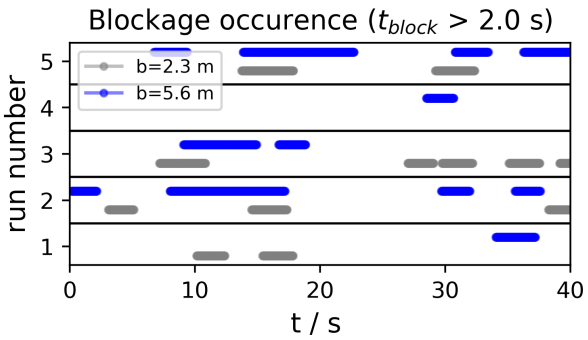

Figure 4.12: Blockage occurrence for N=50 for corridors of width w = 1.2 m and w = 5.6 m

4.2 Variation of number of agents

The filtering of the experimental data set aimed at eliminating influences from the population size. However, the author considers a variation of this initial condition to be useful as well. Based on the standard simulation set with different widths, two variations in the form of N = 25 and N = 75 with constant initial densities are done.

4.2.1 Voronoi densities and blockage occurrence

Reading out Voronoi densities for different population sizes at specific widths, as represented in figure 4.13, several observations can be made. First, the narrowest corridor does not show any changes at all. This makes sense, given the fact that a stable queue can form and persist.

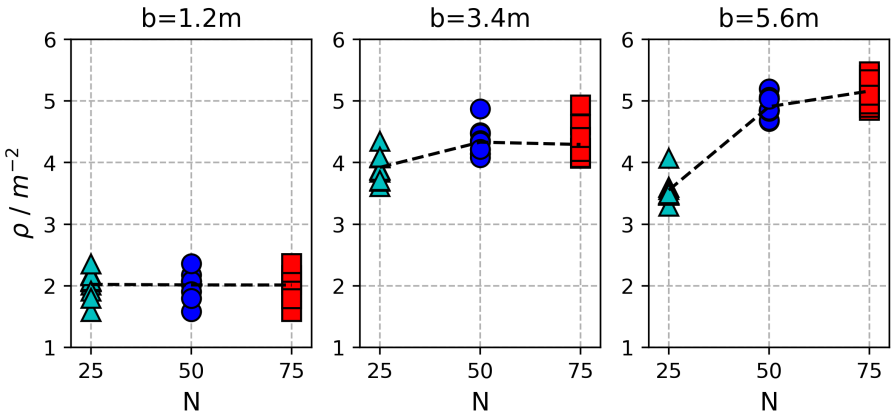

Figure 4.13: Influence of number of agents (N=25, N=50, N=75) on the density in front of the bottleneck for different widths w = 1.2 m, w = 3.4 m and w = 5.6 m

For wider corridors, a general density increase can be seen with a population size increase. However, for the corridor of width w = 3.4 m, the mean density for N=75 is lower than for N=50. This could be due to a runaway value for N=50, so that more simulations would actually result in a horizontal line between N=50 and N=75. Furthermore, comparing N=25 for all widths, the resulting density first augments but then decreases again. This observation is evidence for the importance of arrangement: 25 agents in a corridor width w=3.4 m are still able to build up longer queues, whereas in the widest corridor these are rather short as most of the agents arrive from both sides.

The resulting width-density curves for N=25 and N=75 are shown in figure 4.14. Higher densities are reached for a population size of N=75. Furthermore, the density

maxima for N=25 are achieved earlier, whereas they are delayed for N=75 in comparison to N=50.

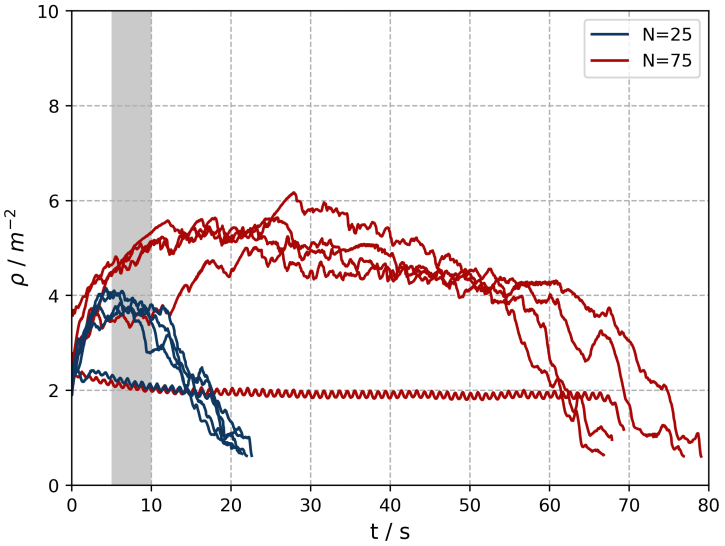

Figure 4.14: Time density series for N=25 and N=75 with early and delayed maxima

As observed in the section before, blocking occurs in wider corridors for N=50. However, the variation of the population size shows that the blocking occurrence changes too. For N=25, the number of blocking stages seems to be less when considering the reduced amount of time. For N=75, the blocking occurrence seems to be reduced as well.

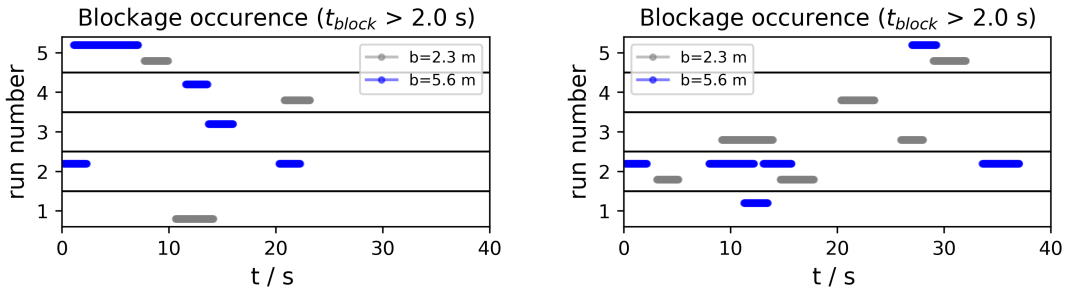

(a) N=25 **(b)** N=75

Figure 4.15: Blockage occurrence for N=25 and N=75

The results show that there is an interference between blocking, population size and the resulting density change. To further study this, a specific test scenario is set up.

4.2.2 Test scenario for model behaviour

The test scenario is designed one-dimensionally to eliminate the influence by e_0 and the first agent is given a desired velocity $v_0 = 0$ m/s. This front agent is comparable to a blocking or clogging situation provoking a jam. The spacing between the idle agent in front of the exit and a second agent approximating is then measured. The number of agents behind the second agent is augmented continuously. The spacing should supposedly be constant irrelevant of the number of agents. The general setup is shown in Figure 4.16.

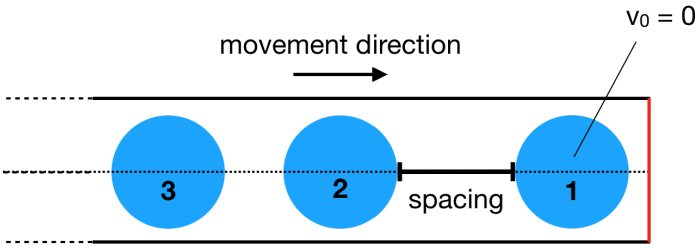

Figure 4.16: One-dimensional test scenario to analyse the influence of number of agents on spacing behaviour between second and first agent with $v_0 = 0$ m/s

Analysing the distance for a case of 2 agents and 10 agents, the distance behaviour with only e_0 activated will be the same. However, the distance behaviour with repulsion activated shows a major difference. For lack of space, these plots are shown in the appendix figure D.5.

In the simulation, different number of agents result in a decrease of the spacing between the idle and second agent. Thus the in-between spacing decreases from 0.16 m for 1 more agent to 0 m for 6 more agents as can be seen in Figure 4.17. The reason for this model behaviour is not known, but could be linked to the summation term for calculating the moving direction e_i. Further investigation is necessary. This simulation behaviour is however responsible for augmenting the density in wide corridors as shown in figure 4.13 when the number of agents is high enough to produce blocking. In a narrow corridor, there will be no blocking or clogging because a stable lane configuration can be established.

It should be kept in mind that this effect could blur the observed density increase for the width variation done previously, so that it is actually overestimated. Nevertheless, even if this simulation behaviour was not intended to be implemented, it seems to reproduce the experimental observation with higher motivation well, making it highly usable for further modelling.

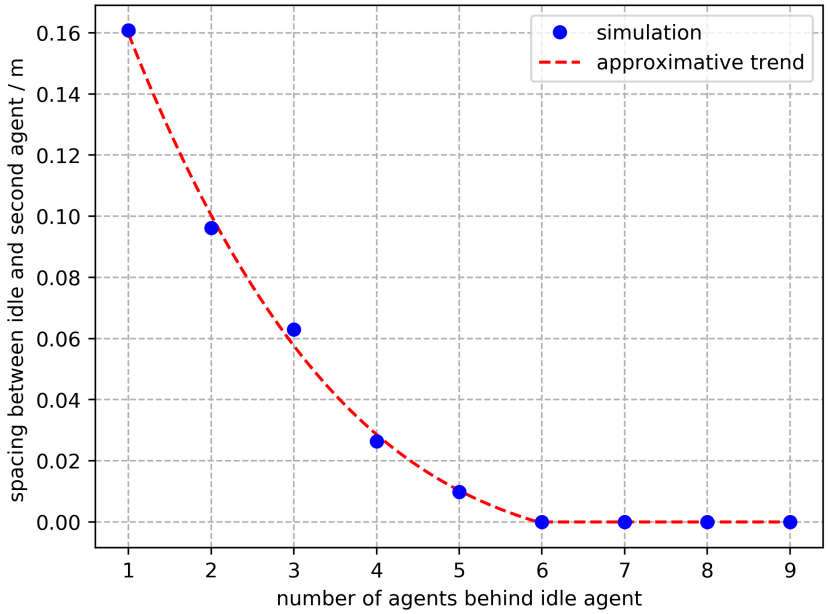

Figure 4.17: Spacing between idle agent in front of the exit and second agent for different N

4.3 Variation of motivation

The occurrence of pushing seems to go hand in hand with a higher motivation. As the goal of this thesis is not to model the behaviour of pushing, alternate ways are searched for to reproduce the experimental dynamics to understand them more. In that context, this section presents the variation for the repulsion parameters a and D, which are calibrated at default with a = 5.0 and D=0.10. From there on, a variation of the time gap parameter T is made. The resulting approach is then applied to simulate one highly motivated crowd respectively two groups with different motivations.

4.3.1 Calibration parameters a and D

Based on the standard parameter set, the repulsion rate a and repulsion distance D of the operational model are both reduced and augmented and all permutations calculated. The identical calibrated parameters for walls are kept at default. Every parameter set is calculated for 5 different runs with their respective seed. Figure 4.18 shows a condensed plot for a total of 9 variations and their influence on the width-density relation.

Generally, it can be seen that the variety in achieved densities is higher for wider corridors. Furthermore, a and D produce opposite results depending on the corridor

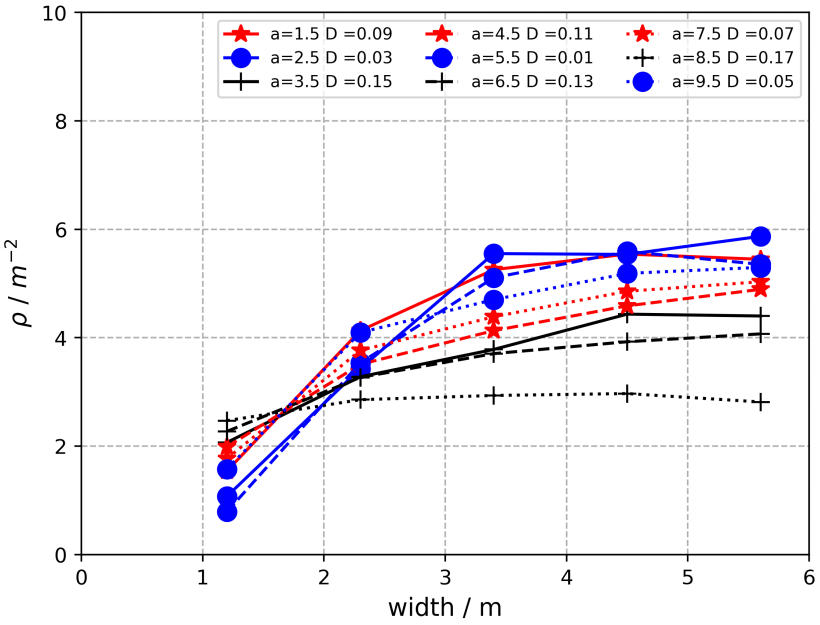

Figure 4.18: Variation results for a and D with intersection between width w = 1.2 m and 2.3 m

width: whereas the smallest values of a and D produce the highest densities in the widest corridor, the exact same values produce the lowest densities in the narrowest corridor.

By consequence the different width-density curves intersect. The intersection or even pivot point of the curves is situated at around 1.6 - 2.0 m. This intersection may indicate a primary impact disappearing, namely the impact of walls. This results in a translation in configuration and thus the model behaving differently with identical calibration parameters. This could be extended to the interpretation of a queuing configuration changing into a clustering configuration between the two widths of w = 1.2 m and w = 2.3 m. However, there are other intersection points inside a specific parameter set at different locations, so that this interpretation should be dealt with caution.

This analysis makes clear that recalibrated a and D parameters have to be used to reach high density states. In concrete terms, the model calibration parameters have to be utilized in certain domains to specifically produce such conditions.

4.3.2 Time gap parameter T

This variation focuses on the time gap parameter T, from which values of $T < 1\ s$ should show a faster contraction. Extreme reduction of the time gap T will result in a maximum agent speed of 1.2 m/s. Moreover, no variance is used so that all agents get the exact same parameter value. This is necessary to get a comparable modelling approach to pushing by making every agent use the process of moving up.

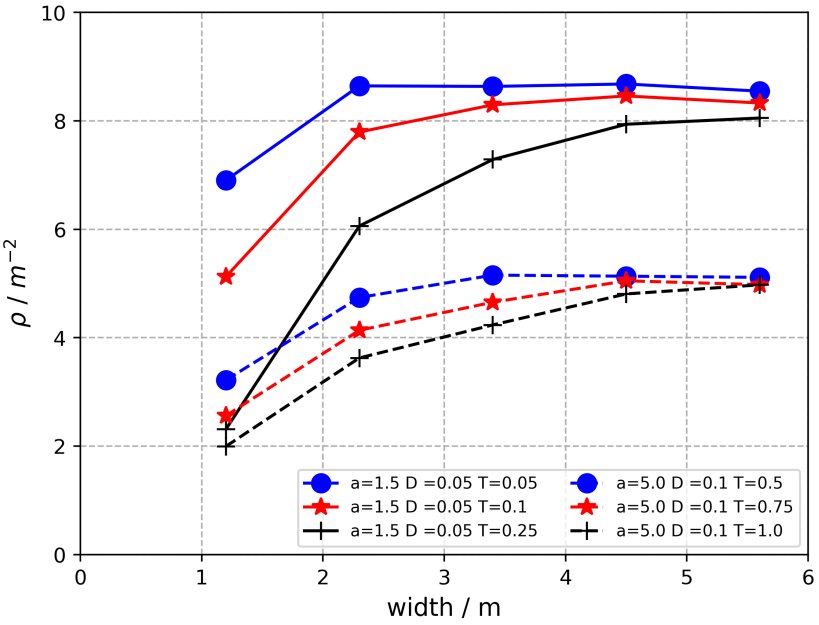

Figure 4.19: Variation results for T, all curves showing initial bend

During a first variation of T, the calibration parameters a and D are kept at default stage. Figure 4.19 shows that a successive reduction of T increases the density in narrow corridors. Densities in narrow corridors can even become higher than in wide corridors when $T < 0.5\ s$ as profound model instabilities arise. In a second variation run, recalibrated a and D values are used in accordance with the section before to reach higher densities. Thus, a fast contracting high density stage in the form of one highly motivated crowd can be simulated. This is illustrated in appendix figure D.6.

From figure 4.19, it can however be seen that T needs to be reduced significantly more to get density increases for the smaller corridor widths. For example, only T=0.05 s will result in 3 agents side by side in the narrowest corridor. However, all curves from the generated runs show a bend for narrow corridors: the density reached is always inferior to that of the wide corridors.

4.3.3 One motivated crowd vs. two types

It is recalled that the simulation of this fast contracting stage is a very artificial scenario, which results in permanent blocking. The used parameter set is T = 0.05 s, a =1.5 and D = 0.05, which is globally used without any variance meaning that all agents behave identical. A look at the Voronoi plots in figure 4.20 for t= 5 s shows an augmentation of the high density area for increasing corridor width and gives an interesting insight for observing lower densities in the narrow corridor.

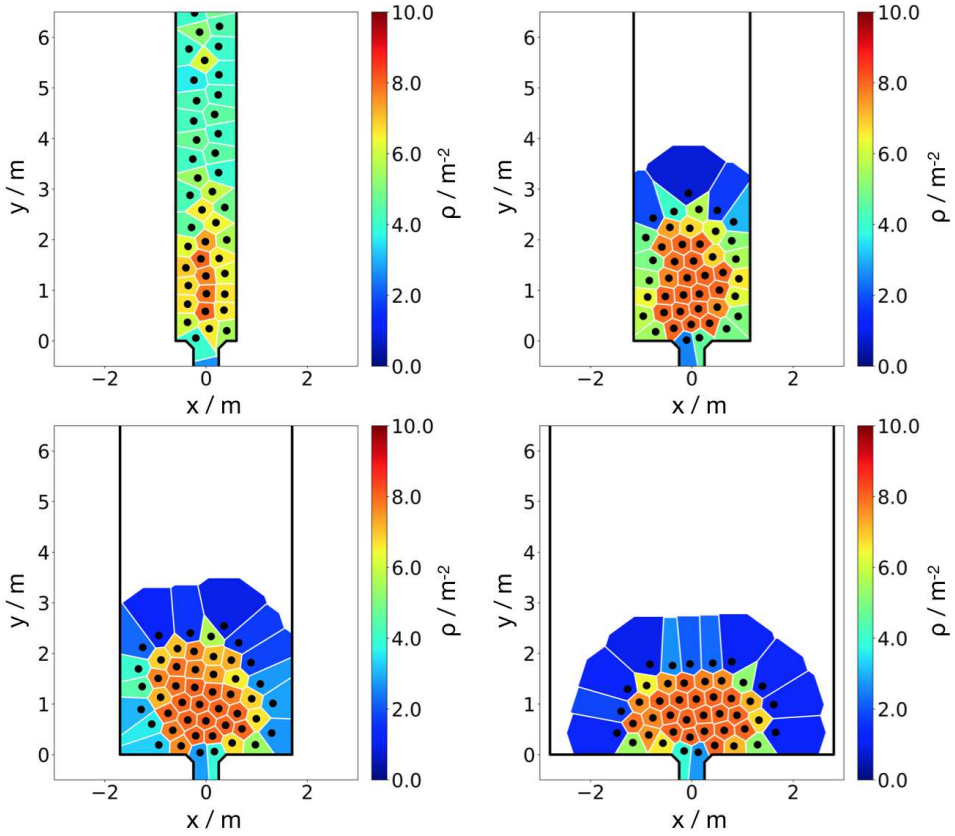

Figure 4.20: Voronoi plots for t = 5s for four corridor widths. The boundary effect is high in the narrow corridor whereas it is obsolete in the wider corridors. Parameters used are N=50, a=1.5, D=0.05, l=0.35, v_0=1.2 and T=0.05. The high density area also increases with increasing corridor width.

In fact, the middle lane in the narrow corridor is nearly at maximum density, however the two side lanes are not. These lanes cannot be additionally contracted as walls instead of agents restrict their available area. The space around these walls isn't used as effectively. Furthermore, the direction of contraction is directed vertically via the exit, which makes it even more improbable to contract horizontally. In the wide corridor,

mobile lanes of agents replace the walls. These can actually have an effect on the Voronoi cells of the middle lanes 2 and 3, ultimately reducing their individual cell size. This synthetic scenario gives a good explanation for the initial bend of the high motivation curve: the boundary effect of walls in the narrow corridor is proportionally higher. It happens in the wide corridor as well, but it has no impact on the measurement area in front of the bottleneck. It is also referred to section 3, which mathematically shows the density difference between a squarish Voronoi and a hexagonal Voronoi cell.

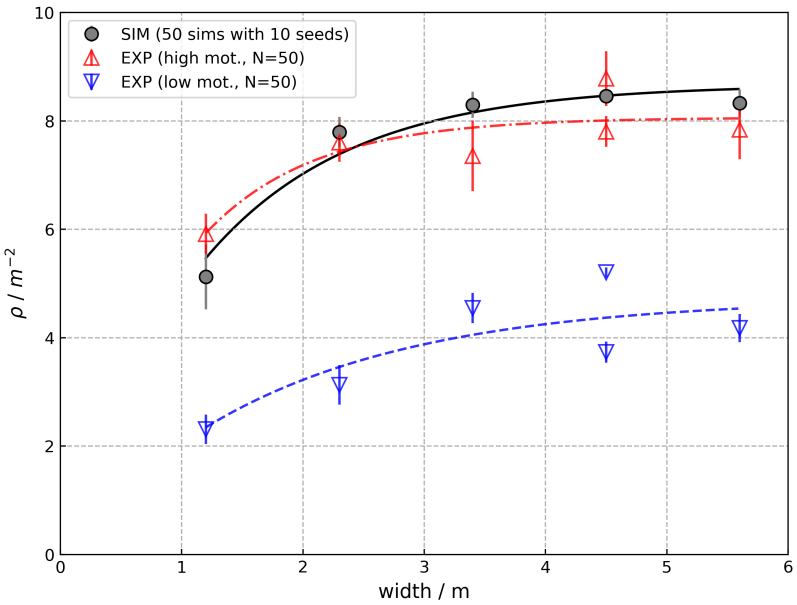

Figure 4.21: Condensed width vs. density plot. The blue and red lines represent the experimental data for low and high motivation, whereas the grey line is the simulation result with the parameter set N=50, a=1.5, D=0.05, l=0.35, v_0=1.2 and T=0.1

A synthetic fit of the experimental width-density curve is possible with the given parameter set and shown in figure 4.21. The density readout fits the width-density data from the experiment optimally, again the narrowest corridor showing the lowest density. However, taking a look at the simulated trajectories, this fit is not very realistic as the generation of time density series as well as distance and time to target plots is not possible due to permanent blocking occurring rather fast. The latter may be the underlying reason that the density can build up so high and persist.

One reason for this blocking could be that all agents have the same parameters, which is unsolvable by the model when symmetric conditions appear. As the simulation results are fogged by this blocking state, an alternative simulation approach is done. One possibility of solving this is the generation of two groups with respect to T. This is

backed up with the knowledge that the experiment shows two types of people too.

Simulations with 2 groups of different T values and a=1.5 reduce the blocking, but it is still significant so that a=1.5 seems to be too restrictive and could as well be the reason for blocking. Thus recalibrated repulsion rate values are used by defining the lowest repulsion rate value as a= 2.5. Thus, two final groups are defined: one having a small time gap T=0.1 and a low repulsion rate a=2.5 and the other group having a high time gap T=1.0 and the standard repulsion rate a = 5.0. The resulting time-density series in figure 4.22 are blocking-free and begin to look like those from the experiment. Furthermore, Voronoi cell plots showing very individual Voronoi cells (c.f. appendix figure D.8) and not one big cluster as well as distance vs. time to target plots are able to be produced. This basically shows that the experimental runs can be reproduced to some extend by changing the motivation approach selected in this thesis.

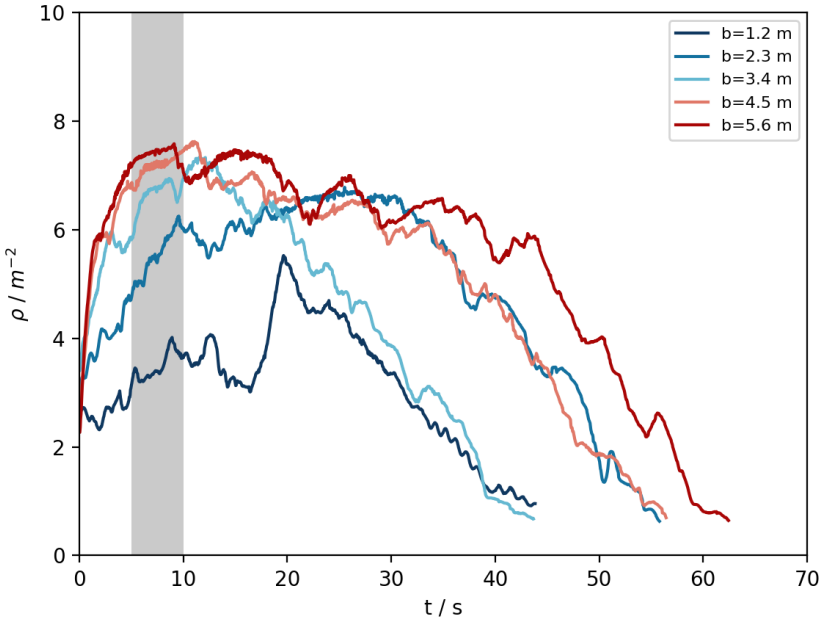

Figure 4.22: Time-density series for N=50, a=2.5/5.0, D=0.05, l=0.35, v_0=1.2 and T=0.1/1.0.

Looking at snapshots from the simulation in figure 4.23, it is however clear that in this specific run the narrow corridor is not able to build up the equivalent density. Highly motivated agents are purely jamming behind the lowly motivated ones as they are not being able to push. Interestingly this is not significant for the wide corridor where the density can build up rather good without the modelling of pushing. A cluster occurs as this state of the system is simple to reach. This shows again the significant effect of boundary conditions. In the narrow corridor, there is also just a density peak

reached, whereas in all other corridor widths the maximum density is maintained during a certain period of time as indicated in figure 4.22.

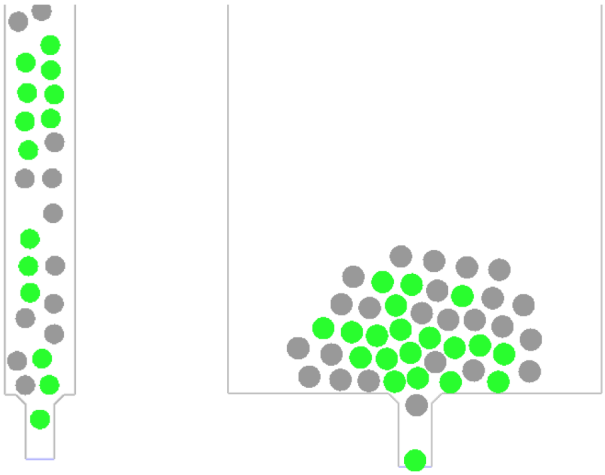

Figure 4.23: JPSvis snapshots for simulating two types of agents, green agents being highly motivated ones. In the narrow corridor, highly motivated agents are purely jamming behind the lowly motivated ones as they are not being able to overtake or even push them. This is not significant for the wide corridor where the density can build up rather good in the form of a cluster given overtaking possibilities, but without pushing modelling.

In a further time-density analysis, two different situations in a corridor width of 1.2 m are provoked. Two seeds are selected in the way that they facilitate overtaking behaviour or actively inhibit it by either placing lowly motivated agents isolated or in groups side by side. The latter will make overtaking much more difficult as units of two lowly motivated agents serve as plugs in the corridor, whereas isolated lowly motivated agents are easy to overtake. Illustrating snapshots can be found in the appendix figure D.7. The two resulting time-density series can be seen in figure 4.24 together with the reference case from the above figure 4.22. The run with high overtaking possibility now shows comparable behaviour to that of the other corridor widths with a stationary density state, whereas the run with no overtaking opportunity postpones the density peak to about t= 30 s. It is important to note that these differences in dynamics can only be grasped when looking at the entire time-density series.

Besides time-density series, significant differences for this high motivation approach can be seen within the agents' trajectories. Therefore, condensed trajectories with low opacity are produced again and are represented for narrower widths in figure 4.25.

The down scaling of the time gap parameter T, which is a time scale reduction of the contraction, lets the ordered structures in the lower part of the more narrower corridors

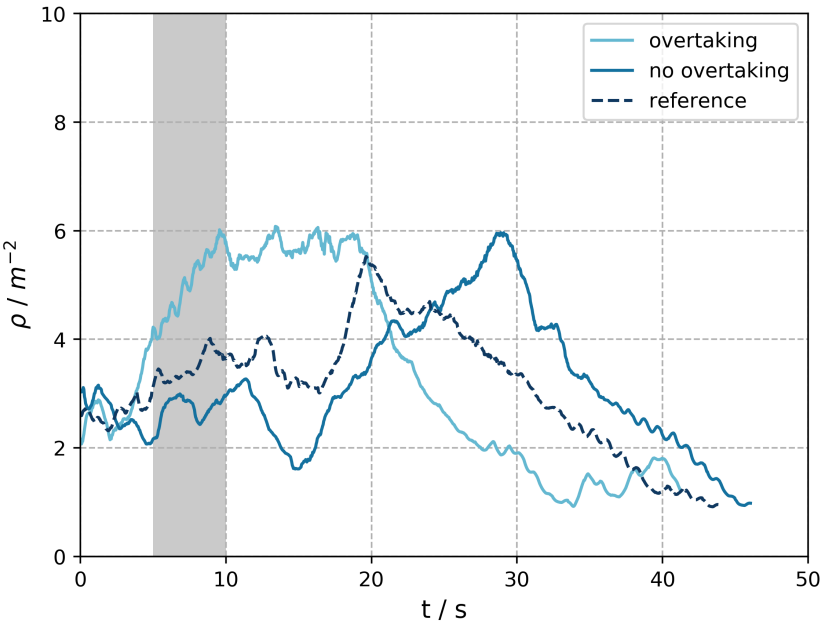

Figure 4.24: Time density series for 3 runs with N=50, a=2.5/5.0, D=0.05, l=0.35, v0=1.2 and T=0.1/1.0. The possibility of overtaking lowly motivated agents results in comparable time density series as for other corridor widths. Inhibiting overtaking postpones this density increase, resulting in a jam of highly motivated agents, which shortly peaks in density right before the exit.

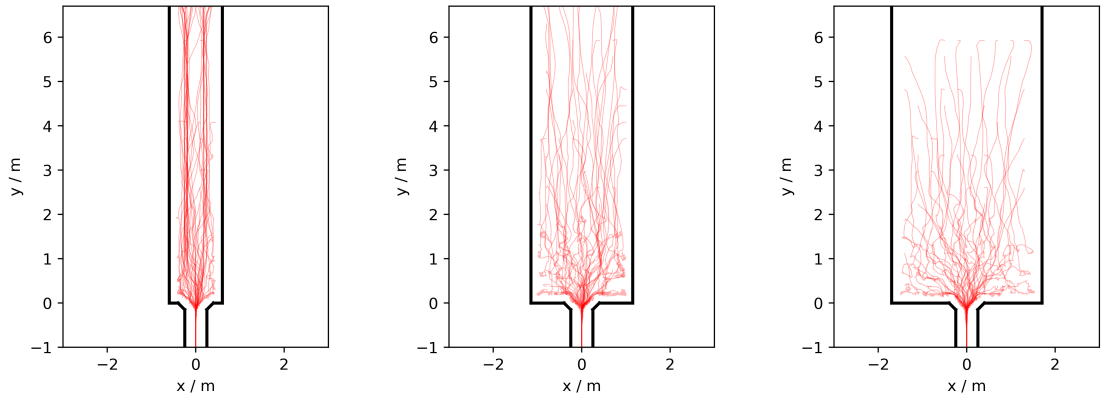

(a) w=1.2 m **(b)** w=2.3m **(c)** w=3.4m

Figure 4.25: Spatio-temporal patterns for narrow corridor widths from condensed low opacity trajectories. A reduction of the contraction time by the time gap parameter T lets the ordered structures in the lower part of the corridors disappear.

disappear. A significant impact by this reduction on the more wider corridors is not seen. Thus, a smaller fill or in this case "moving up time" dissolves a lane configuration into a star-like one, showing that the aspect of time scales is important.

Furthermore, relevant distance to target vs. time to target plots can be found in figure 4.26. By simulating two types of agents, the simulation analysis is able to show that highly motivated agents travel more effectively through space. This can be shown in a demonstrative way in a wide corridor (c.f. figure 4.26b), where nearly all highly motivated agents at the beginning show courses parallel to the x-axis (space component) whereas lowly motivated ones at the beginning show courses parallel to the y-axis (time component). The latter have to wait from the beginning onwards and are thus much more stuck in time.

What's more, the linear relation for all agents observed in the narrow corridor for low motivation only holds up for highly motivated agents in this case (c.f. figure 4.26a). Two types of agents result in differences in times to travel through the corridor. Thus, the courses are staggered. Lowly motivated agents even sometimes have to wait right before the exit as highly motivated ones shove into place.

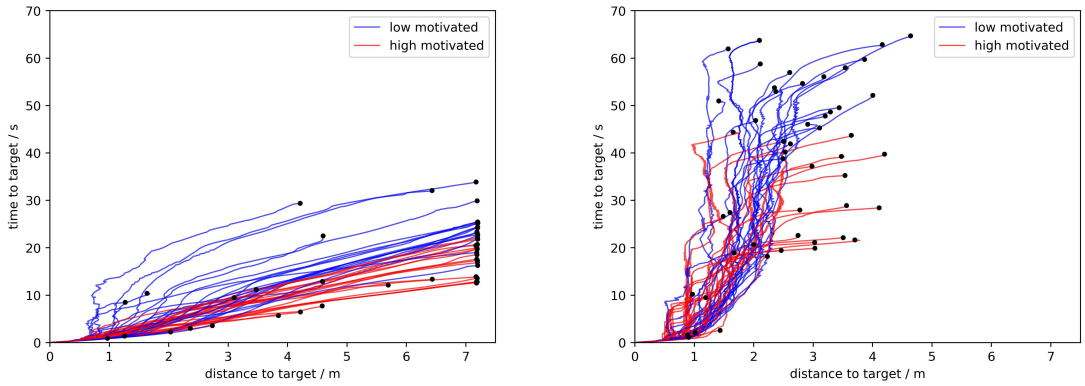

(a) w=1.2 m **(b)** w=5.6m

Figure 4.26: Distance to target vs. time to target plots for two types of agents. The linear relation in the narrow corridor only holds up for highly motivated agents shoving into place so that lowly motivated ones have to wait. In a wide corridor, highly motivated agents show courses parallel to the x-axis at the beginning whereas the courses of lowly motivated ones are parallel to the y-axis (time component).

4.4 Discussion

4.4.1 Simulation outcome with low motivation

The simulations show that different corridor widths result in different trajectory patterns. According to the simulations realised, the density increase for low motivation and comparable to normal circumstances is due to a transfer from a lane into a cluster configuration due to changing the placement of corridor walls. This enlargement ultimately is a change in dimensionality, a transfer from a nearly 1-dimensional narrow corridor to a 2-dimensional wide corridor by a different arrangement of the side walls. Basically, the boundary conditions are changed and allow the below-mentioned factors to arise.

The position of the walls affect the initial desired and moving directions of the agents, their possibility of space filling and overtaking as well as the blockage occurrences in front of the bottleneck. All these factors can actually be summed up as interaction and negotiation issues [11] from which concurring results. This behaviour is rather small in a narrow corridor, but becomes evident in larger ones. This is further supported by the successive change of the x-component concerning the agents' desired direction. With increasing width, more agents simultaneously access the same area in front of the bottleneck.

Primarily the fact that two agents take up the total width in a narrow corridor, making it impossible for other agents to pass them, will finally result in static lanes in a narrow corridor, but dynamic lanes with short lifespan in the wider corridors. It is commonly observed that the distance pedestrians keep to one another increases with their walking speed. General arguments include the larger space for taking a step and a safe gap to avoid collision [11]. The simulations show this exact behaviour for agents when comparing a narrow and wide corridor.

All together, these phenomena could explain the density increase in front of the bottleneck when enlarging the corridor width for low motivation. However, the model behaviour depicted in section 4.2 blurs these findings, which is indicated by the homogeneous density increase. The model reduces the spacing between agents when there is a jam, which is not intended by the implementation. Furthermore, the blocking occurrence is dependent on the number of agents. These two factors synergize to produce higher densities. However, when the number of agents is small, the probability of clogging or a build-up of higher density is not possible, so that the effect doesn't play in wide corridors. This could be related to initial density distribution as with N= 25, rather no agents will be coming from the back in the wide corridor. This could also

explain why higher densities are reached in a middle wide corridor, where this ratio is higher. Thus the density increase cannot be solely accredited with the factors above, which leaves the exact trend of the width-density relation still open.

4.4.2 Simulation outcome with high motivation

Concerning the density increase for high motivation, which could also represent people being in a hurry or emergency situation, it is important to note that a contracted stage is reached in every corridor. The initial bend in the width-density curve is related to two main issues. Once again the boundary effect of the walls has an impact in the narrow corridor. In the wide corridor this boundary effect does not play inside the measurement area. This reduced efficiency of using space at boundaries, in this case walls, compared to the center of the bottleneck is also reported in [1]. Furthermore, the dimensionality difference allows for the contraction of the agents to take place in only one dimension in the narrow corridor, whereas it is a two-component contraction in the wide corridor. A reduced number of near neighbours for the narrow corridor is important as well.

A synthetic fit with the contracted stage is possible, but doubtful when looking at the trajectories. Therefore a plausible approach, which does not exactly fit the experimental data, in the form of generating two groups with regards to repulsion rate a and time gap parameter T was done. The resulting blocking-free time-density series show that the high density state in wider corridors is not impaired by this change, but that narrow corridor will produce a different output. However, when comparing runs with overtaking and no overtaking possibility in the narrow corridor, a comparable behaviour can be seen in the narrow corridor.

This indicates that a high density state is reachable just as well when highly motivated agents can unfold their potential. In the narrow corridor, a high density is build up when overtaking is possible or postponed to a later stage when more highly motivated agents fill up the corridor. This indicates that in such a configuration the ratio of high motivated agents needs to be rather high. This state would be reached during every run when some kind of propagation was implemented. The need for modelling of pushing is therefore evident. Further interesting analyses would then be variable percentages of both populations, e.g. 70:30 or 20:80 etc.

4.4.3 Suggestions for model extensions

This thesis used a simple approach by moving up agents with no propagation of relevant quantities. Therefore, a general approach for pushing is needed primarily.

Relevant cases need to be defined for when pushing occurs respectively can occur. Generally, pushing is not happening when pedestrians can move at free speed, but when people either want to go faster than their predecessor or get stuck and have physical contact. This differentiation could be done via a velocity difference $\Delta v_{ij} = v_i - v_j$ between a preceding pedestrian i and pedestrian j or a condition for contact at standstill with the spacing being minimal (ϵ), which could be mathematically formulated as:

$$p(v_{ij}) = \begin{cases} \Delta v_{ij} \geq 0 & \text{no pushing} \\ \Delta v_{ij} < 0 & \text{pushing} \\ v_i = 0 \text{ with } s_{ij} = \epsilon & \text{pushing} \end{cases}$$

Furthermore, a zone in which the respective agent can unfold his pushing behaviour needs to be determined, which would be limited to the pedestrians in front. This is shown in the left illustration in figure 4.27, where only the relevant agents i, k and l are represented for an agent j.

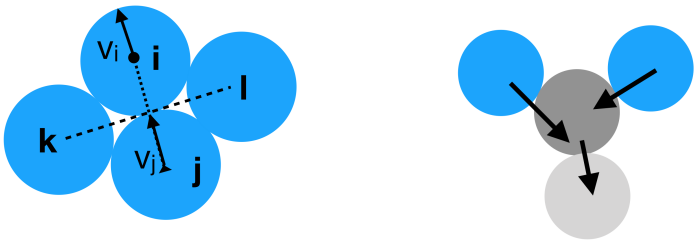

(a) relevant pushing zone **(b)** propagation of pushing

Figure 4.27: Illustrations for pushing modelling. Left: a zone in which the respective agent can unfold his pushing behaviour needs to be determined, which would be limited to the pedestrians in front. Right: propagation of pushing not only influences the agents directly in front, but also agents further away in contact with the agent being pushed

The next step would be to define a way of representing pushing in a velocity-based model. One way could be the imposition of desired velocity of the pushing agent to the agent being pushed. Further modelling accounts for the propagation of this imposition, which could be done via projections of velocities or momentum calculations. This is further depicted in the right illustration in figure 4.27 showing that the pushing behaviour not only influences the agents directly in front, but also agents further away

in contact with the agent being pushed.

Together with this goes the implementation of a desired gap concept, which could also be expressed as a waiting algorithm or a personal space zone in order to better represent queuing behaviour of pedestrians. This desired gap can be intruded into. The algorithm implemented until now is faulty and results in different gaps depending on the number of agents behind the considered agent. Interesting work concerning queuing simulation has been done in [34, 35]. Concerning the desired gap or a personal space zone, [36] gives proposals.

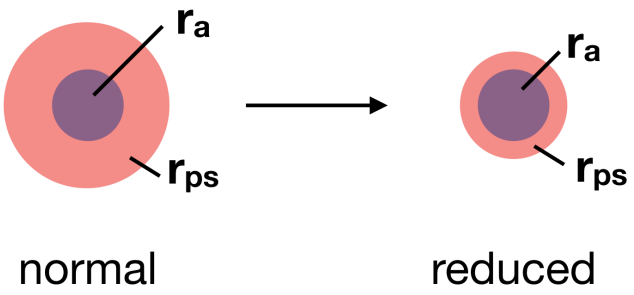

Figure 4.28: Desired gap or personal space zone represented for a normal and reduced case. r_a is the agent's radius and r_{ps} the radius of the personal space zone

Furthermore, the fact that human bodies are deformable to a certain degree should be considered, making their physical boundaries dynamic. This lack of contraction of an agent was solved in this thesis by simulating agents with a smaller agent diameter size l than reported in the literature in order to obtain the maximum densities observed in the experiment.

Finally, it should be thought about an avoiding algorithm next to the repulsion rate a. In detail, two main differentiations need to be made for avoiding: avoiding due to a temporal and spatial relevant collision or desired avoidance for other reasons than collision.

4.4.4 Further analogies to experiments

Concerning the fitted curves, exponential functions do not actually represent satisfactorily what is happening. The high motivation increase is fast and then nearly constant in the simulation and in the experiment for a specific number of participants, more equivalent to a linear jump at the beginning. For low motivation, the change in density is more gradual. Taking this and the other results into account, one could conclude that the narrower corridors bring up a boundary effect. This is more pronounced for lower

motivations, therefore reaching until 3.4 m. In the high motivation case, the boundary effect disappears earlier. Ultimately this seems to be related to the time scale of the contraction, which is different between both motivations and can also be observed in the simulation.

Concerning the runaway values in the experiment, the simulation results offer some interpretation too. The variation of number of agents N in the simulation showed that small populations are not able to equally build up states. This could be an explanation for not seeing density increases for several runs in the experiment [3] even with high motivation. These runs lack a severe density build-up because the number of participants is not sufficient but substantially necessary. On the other hand, a critical number of agents N in wide corridors could possibly result in high densities as reached with high motivation in the experiment as this state can be easily reached without much moving up ("pushing analogy") as shown by simulations. This would explain the experimental data showing high densities in front of the bottleneck with low motivation.

It should be noted that the parameters a and D are actually provoking a shaking of the agents' movement to reach high densities, which could possibly be modelled by using a randomly introduced noise. Interestingly, calibration parameters behave differently depending on the corridor width, the transfer happening between 1.2 m and 2.3 m. The simulation and experiment observed a transfer from queuing to crowding between 1.2 m and 2.3 m as well. Further analyses should investigate if a link can be identified.

For all these findings, it should finally be kept in mind that simplified approaches were used to study these specific pedestrian dynamics. In order to ameliorate and further study the high-density states depicted in this thesis by simulation, it is suggested that further implementations for the used velocity-based model are made and the implementation of some model behaviour reconsidered.

Chapter 5

Conclusion

5.1 Summary

Guaranteeing safety in entrance scenarios is indispensable. Therefore, understanding the arising phenomena in front of bottlenecks is essential. The aim of this thesis was the use of modelling and simulation in order to better understand the differing experimental observations when varying corridor width and motivation of participants in front of bottlenecks. This meant setting up a simulation environment that is able to generate data from a certain modelled behaviour and compare it to the experimental data. As this process should be kept out as easy as possible, an existing velocity-based model was used and its parameters altered to reproduce certain pedestrian dynamics. This included many parameter variations and about a thousand simulations.

In general, the simulations for low motivation deliver interesting insights into the formation of stable lanes and clustering when varying corridor width. The difference between increasing corridor widths relies in progressively different desired directions of agents, which will raise divergence and engender concurring behaviour. Probability of interaction thus rises and negotiation issues result. Furthermore, the narrow corridor does not support overtaking and filling interspace so that it optimizes an unproblematic flow and a higher velocity, whereas in a wide corridor collisions and overtaking are pre-programmed. This is further supported by the simulation results showing no clogging in the narrow corridor, but in all other corridor widths. Specifically, the successive development of the desired direction's x-component with increasing corridor width will produce variability and evolve from a queuing into a crowding situation. The transfer from a nearly 1-dimensional narrow corridor scenario to a 2-dimensional wide corridor scenario due to a different arrangement of the side walls will be accompanied by a density increase in front of the bottleneck. With increasing width, more agents simultaneously

access the same area in front of the bottleneck. The exact trend of this increase is however unclear as an unintentional model behaviour blurs these findings. Thus, further investigation is needed. However, a major density increase seems to happen between corridor widths of 1.2 m and 2.3 m. Moreover, the calibration parameters of the model also behave differently depending on the corridor width, the behaviour of these parameters changing between 1.2 m and 2.3 m corridor width.

The unintentional model behaviour mentioned above is however useful in modelling high motivation situations and utilized accordingly. The simulation results with an increased agent motivation through adapted calibration and agent parameters show a fast contracting stage during which the ordered structures such as stable lanes seen in narrow corridors dissolve. For wider corridors, the change is subtle as this unordered stage is much easier to reach and most of the time already accomplished during low motivation. Nevertheless, lower densities in front of the bottleneck will be observed for the narrow corridor due to the occurrence of geometric boundary effects as shown by preliminary analyses. On the one hand, a boundary effect occurs at walls for the narrow corridor and thus influences the maximum density possible. On the other hand, a reduced number of near neighbours for the narrow corridor is observed implying an overall reduced influence from other agents. Furthermore, the dimensionality difference allows for the contraction of the agents to take place in only one dimension in the narrow corridor, whereas it is a two-component contraction in the wide corridor. As a contracted stage is always reached with high motivation, there will only be an initial reduced density in front of the bottleneck for the narrow corridor.

Furthermore, the two-agent-types approach shows that a high-density stage in the narrow corridor is sometimes harder to reach with differing agent behaviour. In the simulation, this was shown through the possibility of overtaking: interspace occurs in the narrow corridor with two types of agents when no overtaking is possible and thus the ratio of highly motivated agents is insufficient for density-build. This never occurs in the wide corridor which always satisfies overtaking. The interspace in the narrow corridor is observed in the experiment as well.

Comparing both the low and high motivation simulations, the time gap parameter T modifying the time scale of contraction, plays a major role in changing the simulation outcome, which is the essential difference in the experiment too. The high motivation density increase is fast and then nearly constant in the simulation and in the experiment for a specific number of participants, equivalent to a linear jump at the beginning. For low motivation, the increase in density is more gradual.

Finally, runaway values observed in the experiment can be explained by some simulation results. The variation of number of agents N in the simulation showed that

small populations are not able to build up equal states due to arrangement. This could be an explanation for not seeing density increases for several runs in the experiment even with high motivation. On the other hand, simulation shows that a critical number of agents N in wide corridors can result in high densities as reached with high motivation in the experiment as this state can be easily reached without much moving up ("pushing" analogy).

5.2 Closing remarks and outlook

The results show that the current modelling approach is able to reproduce observed behaviour in experimental setups. A good accordance is reached and profound explanations given for why the data emerges as it does. However, extensions to the original model like pushing, desired gap and an avoiding algorithm are necessary in order to better describe the resulting dynamics and conduct further analysis such as varying population sizes and impact of initial conditions like initial density in the corridor.

Velocity-based models thus primarily need extensions in order to better represent queuing and crowding phenomena in front of bottlenecks. Meanwhile, other models could certainly be applied to reconstruct the experimental data, among others this would include force-based models like the social force model. One should however consider the loss of advantages from velocity-based models.

Bibliography

[1] Armin Seyfried, Oliver Passon, Bernhard Steffen, Maik Boltes, Tobias Rupprecht, and Wolfram Klingsch. New insights into pedestrian flow through bottlenecks. *Transportation Science*, 43(3):395–406, 2009.

[2] Anna Sieben, Jette Schumann, and Armin Seyfried. Collective phenomena in crowds—where pedestrian dynamics need social psychology. *PLOS ONE*, 12(6):1–19, 06 2017.

[3] Juliane Adrian, Maik Boltes, Stefan Holl, Anna Sieben, and Armin Seyfried. Crowding and queuing in entrance scenarios: Influence of corridor width in front of bottlenecks. *arXiv preprint arXiv:1810.07424*, 2018.

[4] Christoph Ament. Modellbildung, Identifikation und Simulation dynamischer Systeme. 2017.

[5] Mohcine Chraibi, Antoine Tordeux, Andreas Schadschneider, and Armin Seyfried. Modelling of pedestrian and evacuation dynamics. *Encyclopedia of Complexity and Systems Science*, pages 1–22, 2018.

[6] Antoine Tordeux, Mohcine Chraibi, and Armin Seyfried. Collision-free speed model for pedestrian dynamics. In *Traffic and Granular Flow'15*, pages 225–232. Springer, 2016.

[7] Dirk Helbing, Péter Molnár, Illés J Farkas, and Kai Bolay. Self-organizing pedestrian movement. *Environment and planning B: planning and design*, 28(3):361–383, 2001.

[8] Dirk Helbing, Lubos Buzna, Anders Johansson, and Torsten Werner. Self-organized pedestrian crowd dynamics: Experiments, simulations, and design solutions. *Transportation science*, 39(1):1–24, 2005.

[9] Yusuke Tajima, Kouhei Takimoto, and Takashi Nagatani. Scaling of pedestrian channel flow with a bottleneck. *Physica A: Statistical Mechanics and its Applications*, 294(1-2):257–268, 2001.

[10] Takashi Nagatani. Dynamical transition and scaling in a mean-field model of pedestrian flow at a bottleneck. *Physica A: Statistical Mechanics and Its Applications*, 300(3-4):558–566, 2001.

[11] Serge P Hoogendoorn and Winnie Daamen. Pedestrian behavior at bottlenecks. *Transportation science*, 39(2):147–159, 2005.

[12] Winnie Daamen and Serge Hoogendoorn. Experimental research of pedestrian walking behavior. *Transportation Research Record: Journal of the Transportation Research Board*, (1828):20–30, 2003.

[13] Tobias Kretz, Anna Grünebohm, and Michael Schreckenberg. Experimental study of pedestrian flow through a bottleneck. *Journal of Statistical Mechanics: Theory and Experiment*, 2006(10):P10014, 2006.

[14] Maik Boltes, Jun Zhang, Antoine Tordeux, Andreas Schadschneider, and Armin Seyfried. *Empirical Results of Pedestrian and Evacuation Dynamics*, pages 1–29. Springer Berlin Heidelberg, Berlin, Heidelberg, 2018.

[15] Bernhard Steffen and Armin Seyfried. Methods for measuring pedestrian density, flow, speed and direction with minimal scatter. *Physica A: Statistical mechanics and its applications*, 389(9):1902–1910, 2010.

[16] Jun Zhang. *Pedestrian fundamental diagrams: Comparative analysis of experiments in different geometries*, volume 14. Forschungszentrum Jülich, 2012.

[17] Christine A Lindberg et al. The oxford american college dictionary. *New York: GP Putnam's Sons*, 2002.

[18] Gerd Wenninger. *Lexikon der Psychologie: in fünf Bänden. 3. M bis Ref.* Spektrum, Akad. Verlag, 2001.

[19] Markus A Wirtz and Janina Strohmer. Dorsch - Lexikon der Psychologie. 18., überarbeitete Auflage. *Bern: Hogrefe*, 2017.

[20] Colin M Henein and Tony White. Agent-based modelling of forces in crowds. In *International Workshop on Multi-Agent Systems and Agent-Based Simulation*, pages 173–184. Springer, 2004.

[21] Nirajan Shiwakoti, Majid Sarvi, and Geoff Rose. Modelling pedestrian behaviour under emergency conditions–state-of-the-art and future directions. In *31st Australasian transport research forum*, pages 457–473, 2008.

[22] Maik Boltes and Armin Seyfried. Collecting pedestrian trajectories. *Neurocomputing*, 100:127 – 133, 2013.

[23] AU Kemloh Wagoum, Mohcine Chraibi, Jun Zhang, and Gregor Lämmel. Jupedsim: an open framework for simulating and analyzing the dynamics of pedestrians. In *3rd Conference of Transportation Research Group of India*, 2015.

[24] Mohcine Chraibi, Ulrich Kemloh, Liao, caoshuchao, Erik Andresen, and ArneGraf. Jupedsim/jpsreport: v0.8.3, June 2018.

[25] *Physikalische Modellbildung*, pages 77–135. Springer Berlin Heidelberg, Berlin, Heidelberg, 2006.

[26] Takahiro Ezaki, Daichi Yanagisawa, and Katsuhiro Nishinari. Pedestrian flow through multiple bottlenecks. *Physical Review E*, 86(2):026118, 2012.

[27] Dirk Helbing and Peter Molnar. Social force model for pedestrian dynamics. *Physical review E*, 51(5):4282, 1995.

[28] Arturo Cuesta, Orlando Abreu, and Daniel Alvear. *Evacuation modeling trends*. Springer, 2015.

[29] RiMEA. *Guideline for Microscopic Evacuation Analysis Version: 3.0.0*. RiMEA e.V., 2016.

[30] Geoffrey Grimmett, David Stirzaker, et al. *Probability and random processes*. Oxford university press, 2001.

[31] Weichen Liao, Jun Zhang, Xiaoping Zheng, and Ying Zhao. A generalized validation procedure for pedestrian models. *Simulation Modelling Practice and Theory*, 77:20–31, 2017.

[32] Ulrich Weidmann. Transporttechnik der Fußgänger: transporttechnische Eigenschaften des Fußgängerverkehrs, Literaturauswertung. *IVT Schriftenreihe*, 90, 1993.

[33] Boxin Tang. Orthogonal array-based latin hypercubes. *Journal of the American statistical association*, 88(424):1392–1397, 1993.

[34] Gerta Köster and Benedikt Zönnchen. A queuing model based on social attitudes. In *Traffic and Granular Flow'15*, pages 193–200. Springer, 2016.

[35] AU Kemloh Wagoum, A Tordeux, and W Liao. Understanding human queuing behaviour at exits: an empirical study. *Royal Society open science*, 4(1):160896, 2017.

[36] Isabella Von Sivers and Gerta Köster. Dynamic stride length adaptation according to utility and personal space. *Transportation Research Part B: Methodological*, 74:104–117, 2015.

Appendix A

Initial configuration files

A.1 JPS geometry file

```
<?xml version="1.0" encoding="UTF-8" standalone="yes"?>
<geometry version ="0.8" caption="second life" xmlns:xsi="http://www.w3.org/2001/
    XMLSchema-instance" xsi:noNamespaceSchemaLocation="http://xsd.jupedsim.org/
    jps_geometry.xsd" unit="m">
  <rooms>
    <room id="0" caption="hall">
      <subroom id="1" caption="Room 1" class="Not specified" A_x="0" B_y="0" C_z="0">
          <polygon>
            <!-- left barrier !-->
            <vertex px="-0.25" py="-1.10"/>
            <vertex px="-0.25" py="-0.15"/>
            <vertex px="-0.40" py="0.00"/>
            <vertex px="-0.6" py="0.00"/>
            <!-- hinten zu !-->
            <vertex px="-0.6" py="6.70"/>
            <vertex px="-2.6" py="6.7"/>
            <vertex px="-2.6" py="10.7"/>
            <vertex px="2.6" py="10.7"/>
            <vertex px="2.6" py="6.7"/>
            <vertex px="0.6" py="6.70"/>
            <!-- right barrier !-->
            <vertex px="0.6" py="0.00"/>
            <vertex px="0.40" py="0.00"/>
            <vertex px="0.25" py="-0.15"/>
            <vertex px="0.25" py="-1.10"/>
          </polygon>
      </subroom>
    </room>
  </rooms>
  <transitions>
      <transition id="0" caption="NaN" type="NaN" room1_id="0" subroom1_id="1"
          room2_id="-1" subroom2_id="-1">
          <vertex px="-0.25" py="-1.1"/>
          <vertex px="0.25" py="-1.1"/>
      </transition>
```

```
    </transitions>
</geometry>
```

A.2 JPScore file

```
<?xml version="1.0" encoding="UTF-8" ?>

<JuPedSim project="scenario_ben" version="0.8"
    xmlns:xsi="http://www.w3.org/2001/XMLSchema-instance"
    xsi:noNamespaceSchemaLocation="../../xsd/jps_ini_core.xsd">

<!-- header: seed, geometry, output format -->
<seed>1</seed>
<max_sim_time>200</max_sim_time>
<!--maxCPU>1</maxCPU-->

<geometry>0_geo.xml</geometry>

<!-- trajectories file and format -->
<trajectories format="xml-plain" fps="25">
<file location="2_traj.xml" />
</trajectories>

<show_statistics>true</show_statistics>
<logfile>log</logfile>

<!-- agents -->
<agents operational_model_id="3">
    <agents_distribution>
        <group group_id="1" agent_parameter_id="1" room_id="0" subroom_id="1"
            number="3" router_id="1" pre_movement_mean="0" pre_movement_sigma="0"
                y_min="0.0" y_max="1.0"/>
        <group group_id="2" agent_parameter_id="1" room_id="0" subroom_id="1"
            number="3" router_id="1" pre_movement_mean="0" pre_movement_sigma="0"
                y_min="1.0" y_max="2.0"/>
        <group group_id="3" agent_parameter_id="1" room_id="0" subroom_id="1"
            number="3" router_id="1" pre_movement_mean="0" pre_movement_sigma="0"
                y_min="2.0" y_max="3.0"/>
        <group group_id="4" agent_parameter_id="1" room_id="0" subroom_id="1"
            number="3" router_id="1" pre_movement_mean="0" pre_movement_sigma="0"
                y_min="3.0" y_max="4.0"/>
        <group group_id="5" agent_parameter_id="1" room_id="0" subroom_id="1"
            number="3" router_id="1" pre_movement_mean="0" pre_movement_sigma="0"
                y_min="4.0" y_max="5.0"/>
        <group group_id="6" agent_parameter_id="1" room_id="0" subroom_id="1"
            number="3" router_id="1" pre_movement_mean="0" pre_movement_sigma="0"
                y_min="5.0" y_max="6.0"/>
        <group group_id="7" agent_parameter_id="1" room_id="0" subroom_id="1"
            number="2" router_id="1" pre_movement_mean="0" pre_movement_sigma="0"
                y_min="6.0" y_max="6.7"/>
        <group group_id="8" agent_parameter_id="1" room_id="0" subroom_id="1"
            number="30" router_id="1" pre_movement_mean="0" pre_movement_sigma="0"
                x_min="-1.5" x_max="1.5" y_min="6.7" y_max="9.0"/>
```

```
    </agents_distribution>
</agents>

<!-- operational models -->
<operational_models>

    <model operational_model_id="3" description="Tordeux2015">
        <model_parameters>
            <solver>euler</solver>
            <stepsize>0.1</stepsize>
    <periodic>0</periodic>
            <exit_crossing_strategy>3</exit_crossing_strategy>
            <linkedcells enabled="true" cell_size="30" />
            <force_ped  a="5" D="0.1" />
            <force_wall a="5" D="0.02" />
        </model_parameters>
        <agent_parameters agent_parameter_id="1">
            <v0 mu="1.34" sigma="0.0" />
            <bmax mu="0.175" sigma="0.0" /> <!-- this is l/2, assuming peds are
                 circles with constant radius-->
            <bmin mu="0.175" sigma="0.0" />
            <amin mu="0.175" sigma="0.0" />
            <tau mu="0.5" sigma="0.0" />
            <atau mu="0." sigma="0.0" />
            <T mu="1" sigma="0.0" />
        </agent_parameters>
    </model>

</operational_models>

<!-- route choice models -->
  <route_choice_models>
    <router router_id="1" description="ff_global_shortest" />
  </route_choice_models>

</JuPedSim>
```

A.3 JPSreport file

```
<?xml version="1.0" encoding="UTF-8" ?>
<JPSreport project="JPS-Project" version="0.8" xmlns:xsi="http://www.w3.org/2001/
     XMLSchema-instance" xsi:noNamespaceSchemaLocation="http://xsd.jupedsim.org/0.6/
     jps_report.xsd">
    <!-- geometry file -->
    <geometry file = "0_geo.xml" />
    <!-- trajectories file and format -->
    <!-- either a file name or a path location. In the latter case all files in the
         directory will be used-->
    <trajectories format="xml" unit="m">
        <file name="2_traj.xml" />
        <path location="./" />
    </trajectories>
```

```
<!-- give relative path based on the location inifile or give the absolute path-
     -->
<scripts location="/Users/benhein/Workspace/jpsreport/scripts"/>

<measurement_areas unit="m">
    <area_B id="1" type="BoundingBox" zPos="None">
        <vertex x="-0.4" y="0.5" /> <!-- Clockwise -->
        <vertex x="-0.4" y="1.3" />
        <vertex x="0.4" y="1.3" />
        <vertex x="0.4" y="0.5" />
        <length_in_movement_direction distance="2.0" />
    </area_B>
    <area_L id="2" type="Line" zPos="None">
        <start x="-0.25" y="0" />
        <end x="0.25" y="0" />
    </area_L>
</measurement_areas>

<velocity>
    <use_x_component>true</use_x_component>
    <use_y_component>true</use_y_component>
            <!-- The time interval that used to calculate instantaneous velocity
        of ped i [fr] here v_i = (X(t+frame_step/2) - X(t+frame_step/2))/
             frame_step. X is location. -->
    <frame_step>10</frame_step>
</velocity>

<velocity frame_step="10" set_movement_direction="None" ignore_backward_movement="
     false"/>
<!-- frame_step is the time interval that used to calculate instantaneous velocity
 of ped i [fr] here v_i = (X(t+frame_step/2) - X(t+frame_step/2))/frame_step. X is
     location. -->


<!-- Method A (Zhang2011a) Flow and Vel -->
<method_A enabled="true">
    <!-- Time interval used to count the flow [fr] -->
    <measurement_area id="2" frame_interval="100" plot_time_series="true"/>
</method_A>

<!-- Method B (Zhang2011a) Vel and Dens based on Tin and Tout -->
<method_B enabled="false">
    <measurement_area id="2" />
</method_B>

<!-- Method C (Zhang2011a) Classical density and Vel -->
<method_C enabled="false">
    <measurement_area id="2" plot_time_series="true"/>
</method_C>

<!-- Method D (Zhang2011a) Voronoi density and Vel -->
<method_D enabled="true">
    <measurement_area id="1" start_frame="None" stop_frame="None"
         get_individual_FD="false" plot_time_series="true"/>
    <one_dimensional enabled="false"/>
```

```
        <cut_by_circle enabled="true" radius="1.0" edges="10"/>
        <output_voronoi_cells enabled="false" plot_graphs="false"/>
        <profiles enabled="false" grid_size_x="0.20" grid_size_y="0.20"/>
    </method_D>
</JPSreport>
```

Appendix B

Code fragments for two groups

```
...
      int agent_id = ped->GetID();
      if(agent_id%2 == 0){
        ped->SetSpotlight(true);
        T = 0.25; // high mot.
      }
      else {
        T = 1.0; // low mot.
      }
double speed = (spacing-l)/T;
...
```

```
...
double a = 0;
int agent_id = ped1->GetID();
if(agent_id%2 == 0) {
        ped1->SetSpotlight(true);
        a = 2.5; // high mot.
}
else {
        a = 5.0; // low mot.
}
double D = 0.05;
R_ij = - a * exp((l-Distance)/D);
...
```

Appendix C

Parameter variations per width

code	N	a	D	T	l	v_0	setup	s.p.w.
101	50	5.0	0.10	1.0	0.30	1.34	default	10
102	50	5.0	0.10	1.0	0.35	1.20	standard	10
110	25	5.0	0.10	1.0	0.35	1.20	standard	10
120	75	5.0	0.10	1.0	0.35	1.20	standard	10
130	2-9	5.0	0.10	1.0	0.35	1.20	test scenario	/

Table C.1: used parameters for default, standard and test scenario runs

code	N	a	D	T	l	v_0	setup	s.p.w.
140	50	1.5	0.09	1.0	0.35	1.20	aD var	5
141	50	2.5	0.03	1.0	0.35	1.20	aD var	5
142	50	3.5	0.15	1.0	0.35	1.20	aD var	5
143	50	4.5	0.11	1.0	0.35	1.20	aD var	5
144	50	5.5	0.01	1.0	0.35	1.20	aD var	5
145	50	6.5	0.13	1.0	0.35	1.20	aD var	5
146	50	7.5	0.07	1.0	0.35	1.20	aD var	5
147	50	8.5	0.17	1.0	0.35	1.20	aD var	5
148	50	9.5	0.05	1.0	0.35	1.20	aD var	5

Table C.2: used parameters for a and D variation runs

code	N	a	D	T	l	v_0	setup	s.p.w.
150	50	5.0	0.10	1.0	0.35	1.20	T var	5
151	50	5.0	0.10	0.75	0.35	1.20	T var	5
152	50	5.0	0.10	0.50	0.35	1.20	T var	5
153	50	5.0	0.10	0.25	0.35	1.20	T var	5
154	50	5.0	0.05	0.10	0.35	1.20	T var	5
155	50	1.5	0.05	0.25	0.35	1.20	T var	5
156	50	1.5	0.05	0.10	0.35	1.20	T var	5
157	50	1.5	0.05	0.05	0.35	1.20	T var	5
158	50	10.0	0.05	0.10	0.35	1.20	T var	5

Table C.3: used parameters for T variation runs

code	N	a	D	T	l	v_0	setup	s.p.w.
160	50	1.5/5.0	0.05	0.10/0.5	0.35	1.20	2 groups	5
161	50	1.5/5.0	0.05	0.10/1.0	0.35	1.20	2 groups	5
162	50	1.5/5.0	0.05	0.20/1.0	0.35	1.20	2 groups	5
163	50	1.5/5.0	0.05	0.25/1.0	0.35	1.20	2 groups	5
164	50	2.5/5.0	0.05	0.10/1.0	0.35	1.20	2 groups	5
165	50	2.5/5.0	0.05	0.20/1.0	0.35	1.20	2 groups	5
166	50	2.5/5.0	0.05	0.25/1.0	0.35	1.20	2 groups	5

Table C.4: used parameters for 2 types of agents runs

Appendix D

Supplementary material

D.1 Initial density calculation for N=25 and N=75

width (m)	1.2	2.3	3.4	4.5	5.6
$\boldsymbol{N_{cor}}$	20	25	25	25	25
$\boldsymbol{N_{out}}$	5	0	0	0	0
$\boldsymbol{l_{red}}$	/	4.3	3.0	2.2	1.8

Table D.1: Calculated values N_{cor}, N_{out} and l_{red} for 25 agents

width (m)	1.2	2.3	3.4	4.5	5.6
$\boldsymbol{N_{cor}}$	20	39	57	75	75
$\boldsymbol{N_{out}}$	55	36	18	0	0
$\boldsymbol{l_{red}}$	/	/	/	/	5.4

Table D.2: Calculated values N_{cor}, N_{out} and l_{red} for 75 agents

D.2 Desired direction using floorfield

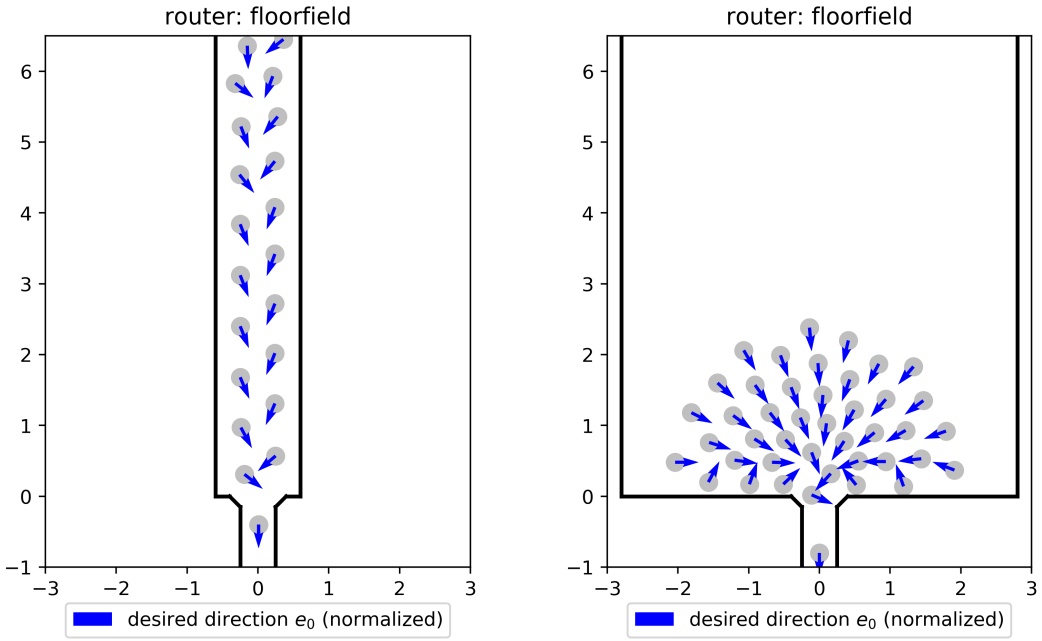

(a) (b)

Figure D.1: emerging desired directions e_0 using global shortest router with floorfield, which is due to the intermediate target calculation

D.3 Square vs. hexagonal Voronoi density

Illustration of density difference between a square and hexagonal area in function of r. A circle with radius r is considered. This fits in a square with a side length $a = 2r$ or a hexagon with a side length $b = \frac{2r}{\sqrt{3}}$, see figure D.2. The area of the square is thus given by $A = 4r^2$ and the area of the hexagon by $B = 2\sqrt{3}r^2$, the respective density by the inverse of these two resulting is an $1/r^2$ relation.

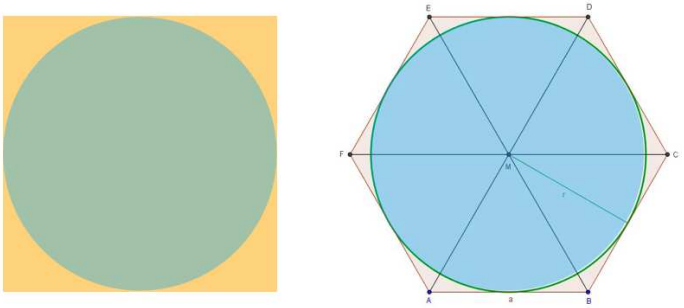

Figure D.2: Area taken by a circle in a square vs. area taken by circle in a hexagon

The difference of both densities is plotted in Figure D.3, showing that a radius in the range of the size of a pedestrian/agent comes along with important density differences.

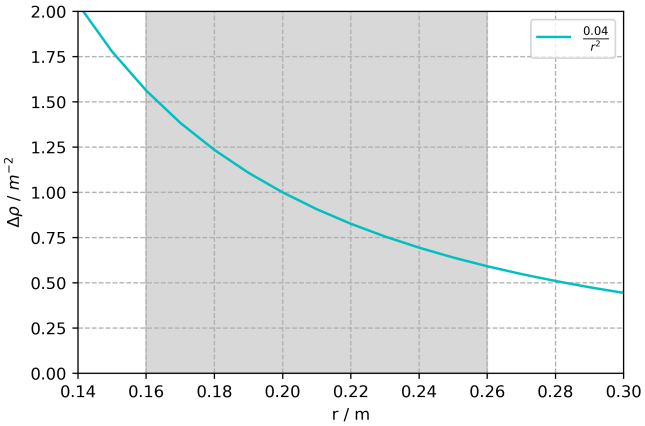

Figure D.3: Density difference between square and hexagon in function of r

D.4 Desired vs. moving direction and impact on spacing

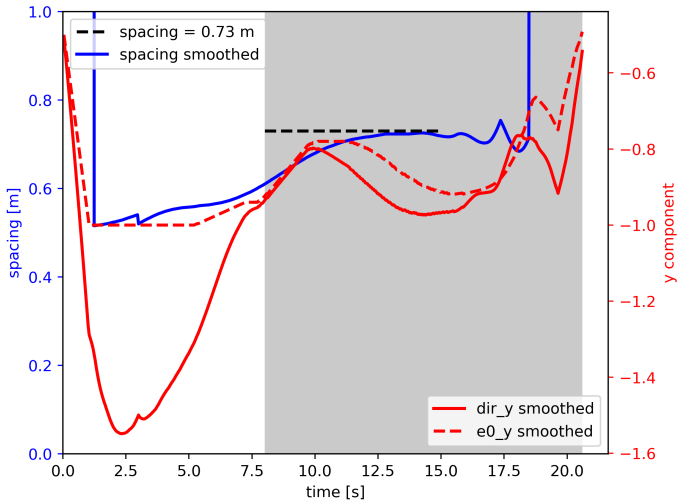

(a)

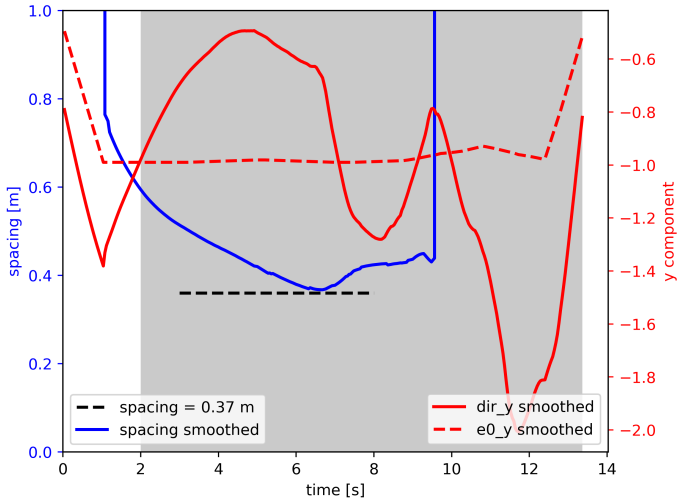

(b)

Figure D.4: Plotting of spacing, desired direction (y-component) and moving direction (y-component) for one representative agent in a narrow and wide corridor. The spacing is clearly higher in a narrow corridor and e_i in small corridors will only differ a little from e_0. In wide corridors, e_i will be significantly different from e_0.

D.5 Test scenario analysis with 2 and 10 agents

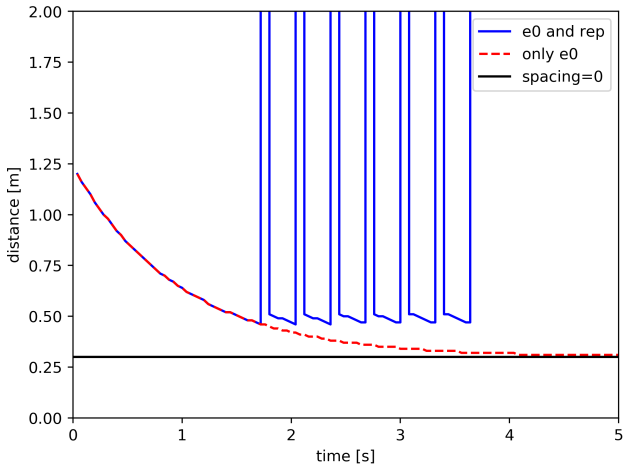

(a) 2 agents (1 + 1 behind)

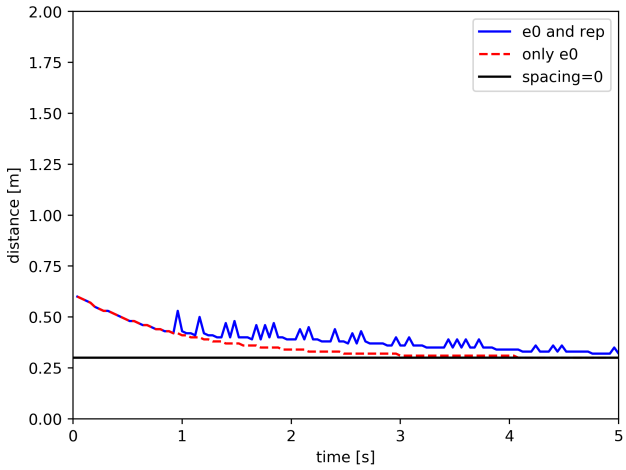

(b) 10 agents (1 + 9 behind)

Figure D.5: Analysing the distance for a case of 2 agents and 10 agents, the distance behaviour with only e_0 activated will be the same. However, the distance behaviour with repulsion activated shows a major difference, the oscillations being high for 2 agents

D.6 Illustrating snapshots for one motivated crowd

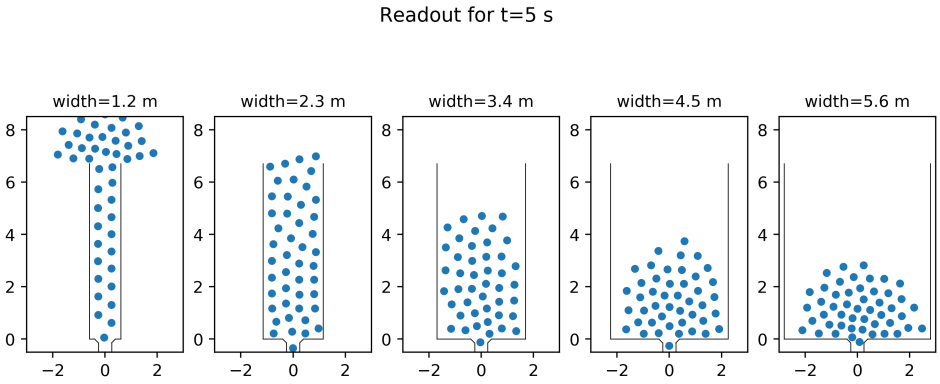

(a) default parameters, low motivation

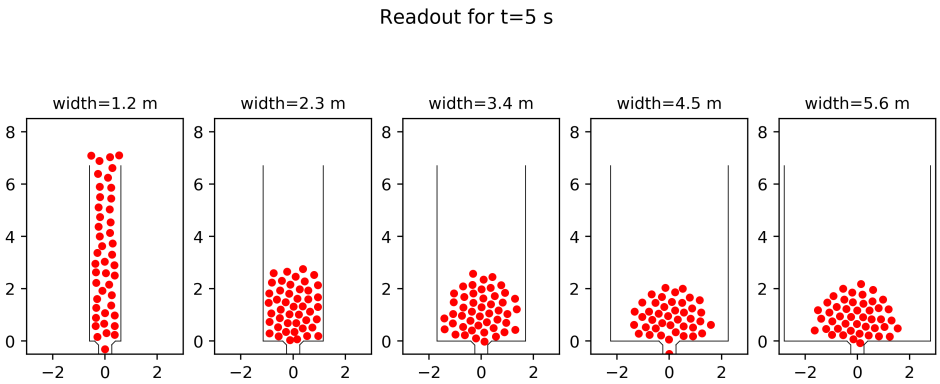

(b) recalibrated parameters a and D and time gap parameter $T \to 0$

Figure D.6: Plots illustrating the low and high density states reached in the simulation to represent a comparable approach to different motivations

D.7 Illustrating snapshots for 2 types of agents

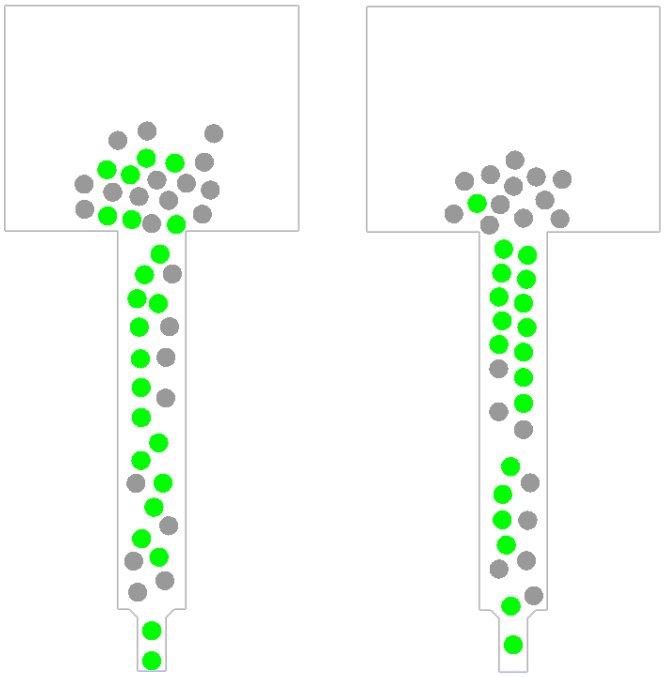

(a) **(b)**

Figure D.7: Simulation snapshots showing overtaking (left) and no overtaking possibility (right). By consequence, a lane of highly motivated agents will develop in the left picture, whereas in the right picture they accumulate behind lowly motivated agents

D.8 Voronoi cells for two types of agents

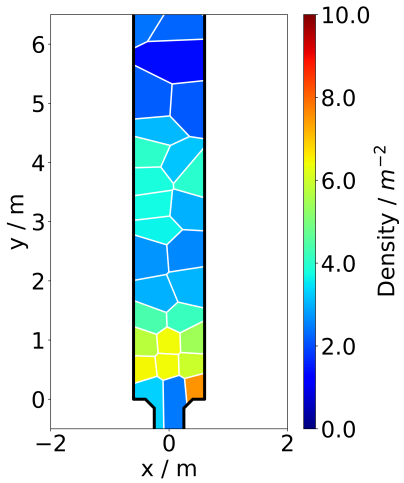

(a) w = 1.2 m

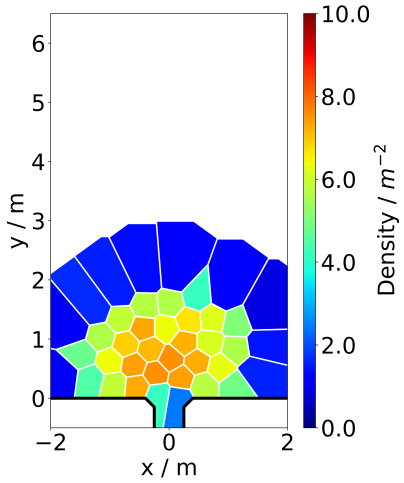

(b) w = 4.5 m

Figure D.8: Voronoi plots for 2 types of agents indicating that higher densities are simpler and faster to reach in a wide corridor

Appendix E

Listing of bash and python scripts

The following python and bash scripts have been written to produce, analyse and plot the data during this thesis:

- master.sh
- auto.sh
- voronoi.py
- smoothed_time_density.py
- plot_dist_wait.py
- data_filter.py
- geo.py
- configs.py
- graphics.py
- r_vs_density.py
- max_neigbours.py
- constant_densities.py
- momentan.py
- master_flow.py
- T_trends.py
- repulsion_functions.py
- latin.py
- several_seeds.py
- change_seed.py
- autoplots.py
- time_densities_seeds.py
- trajectories_plot.py
- directions.py

```
x_component.py
spacing_vs_repulsion.py
dist_wait_standard.py
specific_w_N.py
blockage.py
master_plot_aD.py
master_plot_T.py
```

They can be found in the digital appendix.